CANMET

Canada Centre for Mineral and Energy Technology

Centre canadien de la technologie des minéraux et de l'énergie

Mining Research Laboratories

Laboratoires de recherche minière

Energy, Mines and Resources Canada

Énergie, Mines et Ressources Canada

Canada

THE ENERGY OF OUR RESOURCES · THE POWER OF OUR IDEAS

L'ENERGIE DE NOS RESSOURCES · NOTRE FORCE CREATRICE

Uniaxial and Triaxial Compression Tests on URL Rock Samples from Boreholes 207-045-GC3 and 209-069-PH3

J.S.O. Lau and B. Gorski March, 1992.

Divisional Report MRL 92-025(TR)

This document is an unedited interim report prepared primarily for discussion and internal reporting purposes. It does not represent a final expression of the opinion of the Canada Centre for Mineral and Energy Technology (CANMET)

Ce document est un rapport provisoire non révisé et rédigé principalement pour fin de discussion et de documentation interne. Il ne représente nullement l'expression définitive de l'opinion du Centre canadien de la technologie des minéraux et de l'énergie (CANMET)

52pp

MICROMEDIA

92-06299/

Uniaxial and Triaxial Compression Tests on URL Rock Samples from Boreholes 207-045-GC3 and 209-069-PH3

J.S.O. Lau[1] and B. Gorski[2]

Abstract

Uniaxial and triaxial compression tests were conducted on pink granite core samples obtained at the 240 level of AECL Research's Underground Research Laboratory (URL) to determine the strength and deformation properties of the rock. Two methods were employed, one using the Hoek cell and the other one using the triaxial cell.

The initiation of cracks in the specimens occurred at stress levels approximately equal to 30% to 60% of the peak deviator stresses. The onset of unstable crack growth occurred at stress levels ranging from 53% to 78% of the peak deviator stresses. The peak strength, strength at initial dilation and strength at unstable crack growth were defined and determined for each specimen. Results suggested that the stress required to initiate unstable crack growth might be related to the long term in situ strength of the rock.

The strength of the rock increased with confining pressure. However, confining pressure was found to have little effect on the tangent Young's modulus and the Poisson's ratio of the rock.

Keywords: stress, strain, strength, confining pressure, initial dilation, unstable crack growth, failure envelope, modulus, Poisson's ratio

---

[1]Geotechnical Engineer, AECL Research, on attachment to Canadian Mine Technology Laboratory, Mining Research Laboratories, CANMET, Energy, Mines and Resources Canada, Ottawa, Ontario.

[2]Physical Scientist, Canadian Mine Technology Laboratory, Mining Research Laboratories, CANMET, Energy, Mines and Resources Canada, Ottawa, Ontario.

Essais de compression uniaxiale et triaxiale effectués sur des éprouvettes LRS extraites des trous 207-045-GC3 et 209-069-PH3

J.S.O. Lau[3] et B. Gorski[4]

Résumé

On a effectué des essais de compression uniaxiale et triaxiale sur des éprouvettes de granite rose provenant du niveau 240 du Laboratoire de recherche souterrain (LRS) d'EACL, en vue de déterminer la résistance et les propriétés de déformation de la roche. Deux méthodes ont été employées, une avec la cellule de Hoek et une autre avec la cellule triaxiale.

La fissuration des éprouvettes a commencé à des degrés de contrainte correspondant à peu près de 30 à 60% aux contraintes déviatoriques maximales. La croissance instable des fissures a été amorcée à des degrés de contrainte allant de 53 à 78% des contraintes déviatoriques maximales. La résistance maximale, la résistance au moment de la dilatation initiale et la résistance durant la croissance instable des fissures ont été définies et déterminées pour chaque éprouvette. Les résultats portent à croire que la contrainte requise pour amorcer la croissance instable de fissures pourrait être reliée à la résistance à long terme de la roche en place.

La résistance de la roche augmente en fonction de la pression de confinement. Toutefois, la pression de confinement a peu d'effet sur le module de Young tangentiel et le coefficient de Poisson de la roche.

Mots clés: contrainte, déformation, résistance, pression de confinement, dilatation initiale, croissance instable des fissures, enveloppe de rupture, module, coefficient de Poisson

---

[3]Ingénieur en géotechnique, EACL Recherche, affecté au Laboratoire canadien de technologie minière, Laboratoires de recherche minière, CANMET, Énergie, Mines et Ressources Canada, Ottawa, Ontario.

[4]Chercheur en sciences physique, Laboratoire canadien de technologie minière, Laboratoires de recherche minière, CANMET, Énergie, Mines et Ressources Canada, Ottawa, Ontario.

Contents

Abstract i
RÉUMÉ ii
Introduction 1
Rock Type and Specimen Preparation 2
Test Apparatus and Procedure 3
Hoek triaxial cell 3
Triaxial cell 4
Test Program And Results 5
Discussion 6
Stress and strains observations 6
Rock strength 8
Failure mode 9
Effects of confining pressure 10
Conclusions 10
Acknowledgements 12
References 13

Tables

1. Dimensions, densities and p-wave velocities of specimens from borehole 207-045-GC3 15
2. Dimensions, densities and p-wave velocities of specimens from borehole 209-069-PH3 16
3. Results of uniaxial and triaxial compression tests on specimens from borehole 207-045-GC3 17
4. Results of uniaxial and triaxial compression tests on specimens from borehole 209-069-PH3 18
5. Hoek-Brown failure parameters 19

6. Test method and failure characteristics of specimens from borehole 207-045-GC3 19
7. Test method and failure characteristics of specimens from borehole 209-069-PH3 20

Figures

1. Stress-strain and strain-strain curves for specimen GC3-4.908 21
2. Stress-strain and strain-strain curves for specimen GC3-3.063 22
3. Stress-strain and strain-strain curves for specimen GC3-3.315 23
4. Stress-strain and strain-strain curves for specimen GC3-3.468 24
5. Stress-strain and strain-strain curves for specimen GC3-3.621 25
6. Stress-strain and strain-strain curves for specimen GC3-3.784 26
7. Stress-strain and strain-strain curves for specimen GC3-5.279 27
8. Stress-strain and strain-strain curves for specimen GC3-4.204 28
9. Stress-strain and strain-strain curves for specimen GC3-5.435 29
10. Stress-strain and strain-strain curves for specimen GC3-4.357 30
11. Stress-strain and strain-strain curves for specimen GC3-4.511 31
12. Stress-strain and strain-strain curves for specimen PH3-118.18 32
13. Stress-strain and strain-strain curves for specimen PH3-118.32 33
14. Stress-strain and strain-strain curves for specimen PH3-118.55 34
15. Stress-strain and strain-strain curves for specimen PH3-118.69 35
16. Stress-strain and strain-strain curves for specimen PH3-120.03 36
17. Stress-strain and strain-strain curves for specimen PH3-124.06 37
18. Stress-strain and strain-strain curves for specimen PH3-124.20 38
19. Stress-strain and strain-strain curves for specimen PH3-124.34 39
20. Stress-strain and strain-strain curves for specimen PH3-124.61 40
21. Stress-strain and strain-strain curves for specimen PH3-124.75 41
22. Stress-strain and strain-strain curves for specimen PH3-124.89 42
23. Hoek and Brown failure envelopes for specimens from borehole 207-046-GC3 43
24. Hoek and Brown failure envelopes for specimens from borehole 209-069-PH3 . 44

25. Plots of angle ß versus confining pressure 45

26. Effects of confining pressure on peak deviator stress, Young's modulus and Poisson's ratio 46

Introduction

AECL Research is assessing the concept of disposal of high-level nuclear fuel wastes in a vault located 500-1000 m deep in plutonic rock. As part of its waste management program, AECL Research has constructed the Underground Research Laboratory (URL) in the Lac du Bonnet Batholith, Manitoba, for conducting large-scale geotechnical and hydrogeological investigations. The URL provides a unique opportunity to evaluate characterization techniques and assess modelling capabilities in a representative geological environment (Simmons and Soonawala, 1982; Simmons, 1990). In preparation for the geomechanical investigations, the Canada Centre for Mineral and Energy Technology (CANMET), in conjunction with AECL Research, has conducted laboratory-scale studies of samples from the URL and the surrounding rock to provide data on the mechanical properties of the rock. This information is required by numerical modellers for input into mechanical models and by engineers for the design of the in situ experiments to be carried out at the URL.

As part of the URL characterization program, uniaxial and triaxial compression tests were conducted over a range of conditions, focusing on determining the peak strength of the Lac du Bonnet granite (Annor and Jackson, 1987; Jackson et al., 1989; Lau et al., 1991). Typical Stress-strain relationships obtained from these tests showed the closure of microcracks and the formation of new microcracks during testing. Unstable crack growth in the specimen is indicated by the reversal of volumetric strain from compression to dilation. Martin and Read (in press) suggested that the stress at which new microcrack growth initiates be referred to as the stress at initial dilation, and the stress corresponding to volumetric strain reversal be referred to as the stress at unstable crack growth. They also suggested that the long term in situ strength of the granite is related to the stress at unstable crack growth. The purpose of this testing program is to determine these stresses as well as the peak strength and the deformation properties of the Lac du Bonnet pink granite. It is hoped that the results will give some insight into the long term in situ strength of the granite.

Rock Type and Specimen Preparation

The rock used in these tests is a medium-grained pink granite. Samples were HQ rock cores obtained from borehole 207-045-GC3 (trend/plunge = 296.89°/69.69°) between the downhole depths of 3.0 and 5.5 m, and borehole 209-069-PH3 (trend/plunge = 013.60°/-05.28°) between the downhole depths of 118.0 and 125.0 m, both located at the 240 Level of the URL.

Specimens were prepared in accordance with the procedure described in the Pit Slope Manual Supplement 3-5 (Gyenge and Ladanyi, 1977) and the method suggested by the International Society for Rock Mechanics (Brown, 1981). The end surfaces of each specimens were ground flat to 0.025 mm to ensure that they were parallel to each other and perpendicular to the axis of the specimen. Surface finishing of the specimens was also required to reduce the diameter of each specimen to the nominal diameter of the NX Hoek triaxial cell. This was performed by surface grinding in a lathe.

The dimensions and bulk densities of the specimens are given in Tables 1 and 2. Each specimen is identified by the borehole name and the downhole depth in metres. The mean bulk density of the pink granite specimens from both boreholes was found to be 2.63 Mg/m^3. Specimen lengths and diameters varied from 111.02 to 117.52 mm and 51.38 to 54.87 mm respectively, resulting in length to diameter ratios ranging from 2.07 to 2.19. Tables 1 and 2 also show the zero-pressure p-wave velocity measured for each specimen prior to testing.

In order to catch the moment when new microcrack growth initiates, it is important to ensure that both the axial and circumferential strains are measured accurately. Micro-measurements type EA-06-500B-120 strain gauges were applied on all specimens for the measurement of deformations. Two diametrically opposed axial strain gauges were bonded at mid height to each of the specimens and were connected in series to form a single active gauge. Similarly, two circumferential strain gauges were mounted at 90° to the axial gauges.

Test Apparatus and Procedure

The uniaxial and triaxial tests were conducted in an MTS 815 Rock Mechanics Test System which is a computer-controlled, servo-hydraulic compression machine, consisting of a 2.22 MN rated load cell, load frame, hydraulic power supply, triaxial cell, confining pressure subsystem, test controller, test processor and DEC micro PDP 11/73 computer. The triaxial cell is equipped with three linear variable differential transducers (LVDT's) for the measurement of axial deformations and an extensometer with a circumferential kit attachment (bicycle chain) for the measurement of circumferential deformation. The reader is referred to the MTS Operational Manual (MTS Systems Corp., 1986) and CANMET Division Report MRL 87-33(INT) (Gorski, 1987) for detailed descriptions of the MTS system and its operation.

Hoek triaxial cell

Two methods were used to conduct the triaxial tests. The first method utilised a NX Hoek triaxial cell in conjunction with the MTS system. The Hoek cell, comprised of a steel body fitted with an urethane jacket, two steel end caps and two self-sealing couplings, is designed to apply confining pressure on a specimen. Details about the Hoek cell and its assembly can be found in various papers (Hoek and Franklin, 1968; Franklin and Hoek, 1970) and will not be repeated in this report. The configuration of the apparatus, however, makes it possible to feed electrical leads from the confining chamber to strain bridges so that deformations can be monitored using strain gauges.

To set up the apparatus for triaxial testing, the strain gauged specimen was inserted in the Hoek cell filled with Syltherm 800 heat transfer liquid, and then placed in the MTS system between the load cell and the ram. A platen was placed on top of the specimen and the ram was extended until it touched the top platen. The strain-gauge leads, passing between the specimen and the urethane jacket, were wired in a half-bridge configuration to B & K type 1526 strain indicators connected to the MTS system. The test began by raising the cell pressure (confining pressure) and the axial load simultaneously to the desired test level. The cell pressure was supplied by the MTS confining pressure subsystem connected to one of the couplings in the cell body. The

specimen was then axially loaded to failure at a constant rate of 0.75 MPa/s under computer control. During the test, analog signals from the load cell, confining pressure subsystem and strain indicator were scanned every 3 seconds by the computer. The signals were converted to engineering units and stored on hard disk in the PDP 11/73 computer. Plots of axial stress versus axial strain and axial stress versus circumferential strain were obtained from a DEC LVP16 pen plotter connected to the PDP 11/73 computer.

Triaxial tests could be set up and performed quickly using the Hoek cell. However, extrusion of the urethane jacket through the gap at the end cap holes was experienced at cell pressures above 30 MPa, causing leakage. The MTS triaxial cell, therefore, was used to conduct tests requiring confining pressures exceeding this 30 MPa threshold.

Triaxial cell

Use of the MTS triaxial cell necessitated that the platen for the stack be modified to accommodate the strain-gauge leads. Sealed electrical feedthroughs had to be machined in the platens to avoid intrusion of the confining fluid. Previous feedthroughs were comprised of holes drilled diagonally through the platen and sealed with Conax connectors. However, it was felt that these holes might cause stress variations across the loading platen, and therefore, they were not used for these tests.

To solve the problem, strain gauge leads were embedded in an epoxy-resin (Metalset A4) layer applied to the sides of the loading platen. The hardened epoxy-resin on the platen was then machined smooth, using a machinist's lathe. The stack was subsequently encapsulated in Teflon shrink tubing and placed into the triaxial cell. Strain-gauge leads were connected to B & K type 1526 strain indicators via electrical connectors located at the bottom of the triaxial cell.

The procedures used to conduct the uniaxial and triaxial compression tests conformed with the methods described in CANMET's Pit Slope Manual Supplement 3-2 (Gyenge and Herget, 1977). LVDT's and an extensometer chain were also set up to provide additional data on axial and circumferential deformations. Syltherm 800 heat transfer fluid was used as the confining fluid.

At the beginning of the triaxial test, the confining fluid pressure and the axial load were raised simultaneously to the test level. The specimen was then loaded to failure under computer control at a constant loading rate of 0.75 MPa/s. Analog signals from the load cell, confining pressure subsystem, strain indicators, LVDT's and extensometer were monitored, converted and recorded by the computer as described earlier.

Test Program And Results

Testing took place from August to November, 1991 at Canadian Mine Technology Laboratory, Mining Research Laboratories, Energy, Mines and Resources Canada in Ottawa. The test program consisted of two series of tests, conducted at the confining pressures of 0, 2, 4, 6, 8, 10, 15, 20, 30, 40, 50 and 60 MPa. The program is summarized and the results are presented in Tables 3 and 4. The first series was performed on specimens from borehole 207-045-GC3. The Hoek cell was mainly used in this series, with the exception of three tests (see Table 6) in which the triaxial cell was used. The second series was carried out on specimens from borehole 209-069-PH3. The triaxial cell was used solely for this series (see Table 7).

Data obtained from these tests included axial stress (σ_1), confining pressure (σ_3), axial strain, circumferential strain and volumetric strain. The volumetric strain was computed from the axial and circumferential strains using the following equation:

$$\varepsilon_v = \varepsilon_a + 2\varepsilon_c \qquad (1)$$

where ε_v = volumetric strain

ε_a = axial strain

ε_c = circumferential strain

Results are presented in the forms of stress-strain and strain-strain curves (Figures 1 to 22) constructed by using SigmaPlot computer software. For each test, five curves were plotted: deviator stress ($\sigma_1 - \sigma_3$) against axial strain, ($\sigma_1 - \sigma_3$) against circumferential strain, axial strain against circumferential strain, volumetric strain against axial strain, and also the volumetric strain

deviation against axial strain.

The volumetric strain deviation is the difference between the actual volumetric strain observed in the test and the elastic volumetric strain calculated by assuming that the rock showed ideal linear deformation behaviour. It was determined using the following procedure. For each specimen, the tangent Young's modulus (E_{40}) and the Poisson's ratio, (ν_{40}) at the stress level equal to 40% of the peak deviator stress were first determined from the stress-strain curves as described in previous reports (Lau and Gorski, 1990; Lau and Gorski, 1991). Assuming the behaviour of the rock was perfectly elastic, these values of E_{40} and ν_{40} were used to estimate the linear elastic behaviour of the specimen over the stress range used for testing. The elastic volumetric strain at each stress level was then compared with the actual observed volumetric strain to obtain the volumetric strain deviation.

Discussion

Stress and strains observations

Figures 1 to 22 show the stress-strain and strain-strain characteristics for the pink granite specimens under uniaxial and triaxial compression. Each figure consists of five plots: deviator stress versus axial strain, deviator stress versus circumferential strain, axial strain versus circumferential strain, volumetric strain versus axial strain, and volumetric strain deviation versus axial strain.

The deviator stress versus axial strain curves, in general, may be divided into three regions. The bottom section is characterized by a steadily increasing slope, indicating the closure of microcracks in the specimen. This region diminishes as the confining pressure increases and disappears at confining pressures above 10 MPa. The middle region is nearly linear, approximating linear elastic behaviour. The top region is characterized by a decreasing slope, indicating crack formation, crack growth and sliding on existing crack interfaces.

The deviator stress versus circumferential strain curves are nearly linear from initial loading to

stress levels equivalent to approximately 30% to 40% of the peak deviator stresses. The curves then start to deviate from linear behaviour, indicating the initiation of cracks in the specimens. The slopes of the curves decrease steadily at first, and then rapidly as failure is approached, indicating the development and growth of cracks in the specimens.

The axial strain versus circumferential strain curves are characterized by progressively decreasing slopes. Although an attempt was made to determine Stacey's critical extension strains (Stacey, 1981) from these curves, it was not possible to approximate the critical value of extension strain by drawing two straight lines, as he suggested. However, it is noticeable that the slopes of these curves start to decrease more rapidly at stress levels in the region of 30% to 40% of the peak deviator stresses.

The volumetric strain versus axial strain curves show that the specimens underwent compression and then dilation during testing. In general, the slopes of the curves decrease steadily from initial loading to axial strain levels corresponding to stress levels approximately equal to 53% to 78% of the peak deviator stresses, where the volumetric strains reach their maximum values. After that, the curves reverse in direction, indicating dilation due to the formation and growth of cracks in the specimens. The slopes of the curves increase (in the negative sense) steadily and then rapidly as failure is approached. For each test, the point at which the volumetric strain reaches its maximum value is referred to as the volumetric strain at the initiation of unstable crack growth. The corresponding point on the deviator stress versus axial strain curve is used to define the stress at which unstable crack growth is initiated (see Figs. 1 to 22).

For each test, the volumetric strain deviation is also plotted against the axial strain. This curve may be divided into three regions. The first region shows the closure of microcracks at the beginning of the test, as the slope of the curve decreases steadily with increasing axial strain. The second region is identified by the approximate coincidence of the curve with the horizontal axis, indicating the volumetric strain deviation is close to zero and the behaviour of the rock is nearly linear elastic. In the third region, the curve again begins to deviate from linear elastic behaviour with the slope increasing exponentially as failure is approached. This indicates the development and growth of cracks, resulting in large difference between the elastic and observed

volumetric strains. The point at which a small but noticeable increase of volumetric strain deviation from zero is detected, is referred to as the initial dilation. Again, the corresponding point on the deviator stress versus axial strain curve is used to define the stress at initial dilation (see Figs. 1 to 22). The stresses at initial dilation were found to be approximately equal to 43% to 60% of the peak deviator stresses.

Rock strength

The peak strength, strength at initial dilation and strength at unstable crack growth for each specimen are presented in Tables 3 and 4. These data were used to determine Hoek-Brown failure parameters for those three strengths. The empirical relationship developed by Hoek and Brown (1980) between the principal stresses associated with the failure of a rock is given as follows:

$$\sigma_1 = \sigma_3 + \sqrt{m\sigma_c\sigma_3 + s\sigma_c^2} \qquad (2)$$

where σ_1 = major principal stress at failure

σ_3 = minor principal stress applied to the rock specimen

σ_c = uniaxial compressive strength of the intact rock material in the specimen

m and s are constants

The predicted uniaxial compressive strength of the intact rock material, σ_c, and the material constant, m, were calculated by using the equations suggested by Hoek and Brown (1980). These values, given in Table 5, were used to develop the Hoek and Brown failure envelopes shown in Figures 23 to 24.

Although these specimens were of the same rock type obtained from the same level at the URL, the peak strengths of specimens from borehole 207-045-GC3 were found to be consistently higher than those from borehole 209-069-PH3 at all confining pressures used in this test program, resulting in considerably higher values of Hoek-Brown failure parameters. However, it is interesting to point out that this discrepancy between the peak strength failure envelopes is not

observed in the cases of the strength at unstable crack growth and the strength at initial dilation. This may indicate that the peak strength of the pink granite was affected by differing degrees of sample disturbance, while the strength at unstable crack growth and the strength at initial dilation are not. If this is true, it suggests that the long term in situ strength of the rock should be related to the strength at unstable crack growth, not the conventional peak strength.

Failure mode

The failure characteristics of the specimens are shown in Tables 6 and 7. Axial fractures and cracks developed in the specimens under the unconfined condition and at very low confining pressures. As the confining pressure increased, the failure characteristics changed, with single or conjugate shear fractures developed in the specimens. The inclination (angle β) of the fracture plane with the specimen axis was measured for each specimen. These angles are given in Tables 6 and 7 and plotted against the confining pressure in Figures 25(a) and (b). It can be seen from those figures that the angle β increased with confining pressure. Also plotted are the relationships between the fracture plane inclination and confining pressure, calculated by means of the following equations suggested by Hoek and Brown (Hoek and Brown, 1980):

$$\tau_m = \frac{1}{2}(\sigma_1 - \sigma_3) \tag{3}$$

$$\sigma = \sigma_3 + \frac{\tau_m^2}{\tau_m + m\sigma_c/8} \tag{4}$$

$$\tau = (\sigma - \sigma_3)\sqrt{1 + m\sigma_c/4\tau_m} \tag{5}$$

The angle β is defined by:

$$\sin 2\beta = \frac{\tau}{\tau_m} \tag{6}$$

The solid line uses m and σ_c values corresponding to the peak strength, whereas, the dashed line uses values corresponding to the strength at unstable crack growth. It can be seen that there is a better agreement between the measured and predicted values of angle β when the strength at unstable crack growth is considered.

Effects of confining pressure

The effects of confining pressure on the peak deviator stress, tangent Young's modulus and Poisson's ratio are illustrated in Figure 26. The peak deviator stress was found to increase with the confining pressure. The confining pressure had little effect on the tangent modulus. Only a slight increase in the modulus value with the confining pressure was observed in the plot for borehole 209-069-PH3. The Poisson's ratio was found to vary from 0.27 to 0.40. However, there is no evidence that the confining pressure had any effect on the Poisson's ratio.

The increase of the tangent Young's modulus with the confining pressure at low confining pressure levels, which was commonly observed in compression tests on the Lac du Bonnet grey granite, was not observed in these test on the pink granite. This suggests that the effect of confining pressure on the modulus of the grey granite might be the effect of sample disturbance in the form of stress-induced microcracks, rather than inherent properties of the rock.

Conclusions

The apparatus and procedures to conduct uniaxial and triaxial compression tests on strain-gauged specimens have been developed and discussed in this report. The triaxial test can be carried out using a NX Hoek triaxial cell in conjunction with the MTS system. However, this method is not recommended for confining pressures higher than 30 MPa due to the leakage problem in the Hoek cell. In the second method, the conventional triaxial cell was used. The new technique of imbedding the strain-gauge leads on to the sides of the platen with a thick coat of epoxy-resin proved to be an effective way to bring out the strain-gauge leads from the specimen without drilling any hole through the platen. These tests have provided stress and strain data for the Lac du Bonnet pink granite. From the results, the following conclusions can be made.

The stress-strain (axial) curves from initial loading to peak strength are marked progressively by regions of increasing slope, approximate linearity and decreasing slope. However, the bottom region corresponding to crack closure diminishes with increasing confining pressure and disappears at confining pressures above 10 MPa.

The stress-strain (circumferential) curves and the strain-strain (axial versus circumferential) curves indicate that the initiation of cracks (initial dilation) in the specimens occurred at stress levels approximately equal to 30% to 40% of the peak deviator stresses. The initiation of cracks can also be seen on the stress-strain (volumetric strain deviation) curves, but at higher stress levels approximately equivalent to 43% to 60% of the peak deviator stresses.

The onset of unstable crack growth (volumetric strain reversal) in the specimens appeared to occur at stress levels approximately equal to 53% to 78% of the peak deviator stresses, as shown in the stress-strain (volumetric) curves.

Hoek and Brown failure envelopes were developed separately for the peak strength, strength at unstable crack growth and strength at initial dilation. Using the peak strength failure criterion, the failure envelope for borehole 207-045-GC3 was found to be considerably stronger than that for borehole 209-069-PH3. However, little difference could be found between the failure envelopes for these two boreholes when the failure criteria based on the strength at crack growth and the strength at initial dilation were used. It is suggested that the peak strength of the pink granite could be affected by sample disturbance, but not the strength at unstable crack growth; and the long term in situ strength of the rock might be related to the strength at unstable crack growth, and not the peak strength. However, more study is required to determine whether or not the strength at unstable crack growth can be directly applied as the long term in situ strength of the rock.

There is a better agreement between the measured and predicted values of the fracture plane inclination (angle β) when failure parameters corresponding to the strength at unstable crack growth were used, instead of those corresponding to the peak strength.

The strength of the pink granite increased with confining pressure. However, the confining pressure was found to have little effect on the tangent Young's modulus and the Poisson's ratio.

Acknowledgements

The authors wish to express their thanks to R. Jackson and G.E. Larocque of CANMET for reviewing this report and making several helpful suggestions. Gratitude is expressed to J. Folta of CANMET for the preparation of specimens and for carrying out the compression wave velocity measurements on the specimens.

References

Annor, A. and Jackson, R. (1987) Mechanical, thermomechanical and joint properties of rock samples from the Lac du Bonnet Batholith, Manitoba. *Geotechnical studies at Whiteshell Research Area (RA-3)* (edited by Katsube, T.J. and Hume, J.P.). Divisional Report MRL 87-52(TR), CANMET, Energy Mines and Resources Canada, pp. 49-110.

Brown, E.T. (1981) Rock characterization testing and monitoring, ISRM suggested methods. International Society for Rock Mechanics, the Commission on Testing Methods, Pergamon, p. 211.

Franklin, J.A. and Hoek, E. (1970) Developments in triaxial testing technique. *Rock Mechanics.* Vol 2, pp. 223-228.

Gorski, B. (1987) Post-failure uniaxial strength determinations using a servo-hydraulic test system. Division Report MRL 87-33(INT), CANMET, Energy, Mines and Resources Canada, p. 77.

Gyenge, M. and Herget, G. (1977) Pit slope manual supplement 3-2 – laboratory tests for design parameters. CANMET, Report 77-26, p. 74.

Gyenge, M. and Ladanyi, B. (1977) Pit slope manual supplement 3-5 – sampling and specimen preparation. CANMET, Report 77-29, p. 30.

Hoek, E. and Brown, E.T. (1980) Underground excavations in rock. The Institution of Mining and Metallurgy, London, p. 527.

Hoek, E. and Franklin, J.A. (1968) A simple triaxial cell for field and laboratory testing of rock. *Trans. Inst. Mining & Metallurgy.* Vol. 77, pp. A22-A26.

Jackson, R., Lau, J.S.O. and Annor, A. (1989) Mechanical, thermo-mechanical and joint properties of rock samples from the site of AECL's Underground Research Laboratory, Lac du Bonnet, Manitoba. *Proc. 42nd Canadian Geotechnical Conference*, Winnipeg, Manitoba, October 23-25, 1989, pp. 41-49.

Lau, J.S.O. and Gorski, B. (1990) High temperature uniaxial and triaxial compression tests on URL rock samples from borehole 401-009-HF1. Divisional Report MRL 90-5(TR), CANMET, Energy, Mines and Resources Canada, p. 91.

Lau, J.S.O., Jackson, R. and Gorski, B. (1991) The effects of temperature and pressure on the mechanical properties of Lac du Bonnet grey granite. *Proc. 32nd U.S. Symposium on Rock Mechanics,* Norman, Oklahoma, July 10-12, 1991, pp. 313-323.

Lau, J.S.O. and Gorski, B. (1991) The post-failure behaviour of the Lac du Bonnet pink granite. Division Report MRL 91-103(TR), CANMET, Energy, Mines and Resources Canada, p. 50.

Martin, C.D. and Read, R. (in press) Strength of massive granite around underground excavations. *Proc. 16th Canadian Rock Mechanics Conference,* Sudbury, Ontario, June 15, 1992.

MTS Systems Corporation (1986) Operation manual for 815 rock mechanics test systems. MTS Systems Corp., Minneapolis, Minnesota, U.S.A.

Simmons, G.R. (1990) Introduction to the Underground Research Laboratory. *Proc. Int. Symposium on Unique Underground Structures,* Denver, Colorado, USA, June 12-15, 1990, pp. 63-1 to 63-20.

Simmons, G.R. and Soonawala, N.M. (1982) Underground research laboratory experimental program. Atomic Energy of Canada Limited Technical Record, TR-135, p. 126.

Stacey, T.R. (1981) A simple extension strain criterion for fracture of brittle rock. *Int. J. Rock Mech. Min. Sci. & Geomech. Abstr.* Vol. 18, pp. 469-474.

Table 1. Dimensions, densities and p-wave velocities of specimens from borehole 207-045-GC3.

Specimen Identification	Length (mm)	Diameter (mm)	Bulk Density (Mg/m^3)	P-wave Velocity (km/s)
207-045-GC3-3.063	115.77	52.57	2.63	6.040
207-045-GC3-3.315	116.97	53.96	2.62	5.964
207-045-GC3-3.468	117.21	53.98	2.63	6.086
207-045-GC3-3.621	117.20	53.88	2.63	5.939
207-045-GC3-3.784	117.85	53.77	2.63	6.113
207-045-GC3-4.049	113.98	54.20	2.62	6.074
207-045-GC3-4.204	117.52	53.92	2.63	5.600
207-045-GC3-4.357	115.06	54.87	2.63	6.139
207-045-GC3-4.511	117.27	54.30	2.63	6.093
207-045-GC3-4.908	116.92	53.54	2.62	6.283
207-045-GC3-5.279	114.02	53.87	2.62	6.455
207-045-GC3-5.435	115.84	54.03	2.63	6.360
Mean			2.63	6.096
Standard Deviation			0.01	0.219

Table 2. Dimensions, densities and p-wave velocities of specimens from borehole 209-069-PH3.

Specimen Identification	Length (mm)	Diameter (mm)	Bulk Density (Mg/m^3)	P-wave Velocity (km/s)
209-069-PH3-118.18	113.63	52.74	2.63	4.621
209-069-PH3-118.32	113.72	53.38	2.61	4.602
209-069-PH3-118.55	112.47	51.38	2.64	4.717
209-069-PH3-118.69	114.30	54.02	2.63	4.964
209-069-PH3-120.03	114.49	51.52	2.64	4.776
209-069-PH3-124.06	113.73	53.11	2.63	4.756
209-069-PH3-124.20	111.02	53.61	2.63	4.943
209-069-PH3-124.34	113.22	53.72	2.64	4.640
209-069-PH3-124.47	113.47	53.11	2.64	4.776
209-069-PH3-124.61	113.70	53.25	2.64	4.737
209-069-PH3-124.75	114.77	53.53	2.64	4.776
209-069-PH3-124.89	112.71	53.70	2.63	4.943
Mean			2.63	4.771
Standard Deviation			0.01	0.124

Table 3. Results of uniaxial and triaxial compression tests on specimens from borehole 207-045-GC3.

Specimen	σ_3 (MPa)	E_{40} (GPa)	ν_{40}	Initial dilation				Unstable crack growth				Peak		
				σ_1 (MPa)	Axial strain (%)	Cir. strain (%)	Vol. strain (%)	σ_1 (MPa)	Axial strain (%)	Cir. strain (%)	Vol. strain (%)	σ_1 (MPa)	Axial strain (%)	Cir. strain (%)
GC3-4.908	0	74.34	0.34	108	0.152	-0.040	0.072	131	0.182	-0.053	0.075	220		-0.367
GC3-3.063	2	70.13	0.31	121	0.172	-0.042	0.088	157	0.224	-0.065	0.095	255	0.371	
GC3-3.315	4	67.71	0.39	136	0.200	-0.062	0.076	159	0.234	-0.078	0.078	298	0.447	-0.554
GC3-3.468	6	68.88	0.30	168	0.230	-0.057	0.117	219	0.309	-0.088	0.132	344	0.555	-0.730
GC3-3.621	8	75.20	0.36	165	0.204	-0.060	0.084	199	0.251	-0.081	0.089	368	0.518	-0.703
GC3-3.784	10	70.31	0.27	197	0.262	-0.063	0.137	264	0.364	-0.104	0.157	391	0.610	-0.453
GC3-4.049	15											438		
GC3-5.279	15	68.66	0.32	205	0.263	-0.070	0.123	258	0.342	-0.104	0.134	432	0.611	
GC3-4.204	20	74.76	0.33	220	0.258	-0.074	0.111	286	0.351	-0.114	0.124	471	0.645	-0.652
GC3-5.435	30	74.16	0.30	269	0.303	-0.083	0.138					591		-0.549
GC3-4.357	40	75.08	0.38	284	0.304	-0.099	0.106	354	0.402	-0.142	0.117	593	0.851	
GC3-4.511	60	76.06	0.32	394	0.419	-0.119	0.182	533	0.622	-0.205	0.212	712	0.995	-0.546

Table 4. Results of uniaxial and triaxial compression tests on specimens from borehole 209-069-PH3.

Specimen	σ_3 (MPa)	E_{40} (GPa)	ν_{40}	Initial dilation				Unstable crack growth				Peak		
				σ_1 (MPa)	Axial strain (%)	Cir. strain (%)	Vol. strain (%)	σ_1 (MPa)	Axial strain (%)	Cir. strain (%)	Vol. strain (%)	σ_1 (MPa)	Axial strain (%)	Cir. strain (%)
PH3-118.18	0	70.08	0.27	107	0.173	-0.037	0.100	160	0.252	-0.068	0.117	205	0.329	
PH3-118.32	2	68.96	0.34	125	0.197	-0.053	0.092	147	0.229	-0.057	0.096	234	0.328	
PH3-118.55	4	71.75	0.31	148	0.208	-0.055	0.098	183	0.259	-0.077	0.106	277	0.377	-0.414
PH3-118.69	6	65.39	0.31	145	0.216	-0.056	0.104	168	0.253	-0.072	0.108	280		
PH3-120.03	8	71.90	0.32	154	0.204	-0.057	0.091	198	0.271	-0.085	0.101	287	0.411	
PH3-124.06	10	69.39	0.25	188	0.254	-0.058	0.139	239	0.337	-0.089	0.158	323	0.493	-0.331
PH3-124.20	15	68.26	0.39	192	0.252	-0.081	0.090	203	0.269	-0.089	0.090	373	0.592	
PH3-124.34	20	66.99	0.38	213	0.277	-0.093	0.092	258	0.349	-0.126	0.097	421	0.679	-0.766
PH3-124.47	30	74.79										501	0.749	
PH3-124.61	40	74.85	0.29	284	0.313	-0.074	0.164	373	0.439	-0.126	0.188	563	0.758	-0.602
PH3-124.75	50	71.80	0.31	380	0.449	-0.133	0.183	538	0.718	-0.244	0.231	600	0.866	-0.314
PH3-124.89	60	78.46	0.40	336	0.341	-0.122	0.096	389	0.413	-0.157	0.099	602	0.746	-0.427

Table 5. Hoek-Brown failure parameters.

Borehole	Strength	σ_c (MPa)	m	s	n	r^2
207-045-GC3	peak	270	23.16	1.0	12	0.9624
	unstable crack growth	128	23.70	1.0	10	0.9189
	initial dilation	113	13.34	1.0	11	0.9585
209-069-PH3	peak	230	20.70	1.0	12	0.9588
	unstable crack growth	132	19.39	1.0	11	0.6801
	initial dilation	114	11.88	1.0	11	0.8652

n = number of specimens r^2 = coefficient of determination

Table 6. Test method and failure characteristics of specimens from borehole 207-045-GC3.

Specimen	σ_3 (MPa)	Test method	β (degree)	Failure characteristics
GC3-4.908	0	Hoek cell		axial fractures, cracks
GC3-3.063	2	Hoek cell	22	shear fracture, splays
GC3-3.315	4	Hoek cell	20	fragments, conjugate fracture
GC3-3.468	6	Hoek cell		multiple fragments
GC3-3.621	8	Hoek cell	21	shear fracture, splays
GC3-3.784	10	Hoek cell	21	fragments, conjugate fractures
GC3-4.049	15	Hoek cell	24	shear fracture, splays
GC3-5.279	15	triaxial cell	25	shear fracture
GC3-4.204	20	Hoek cell	25	shear fracture, splays
GC3-5.435	30	Hoek cell		fragments, wedge-shaped ends
GC3-4.357	40	triaxial cell	30	shear fracture
GC3-4.511	60	triaxial cell	30	shear fracture

Table 7. Test method and failure characteristics of specimens from borehole 209-069-PH3.

Specimen	σ_3 (MPa)	Test method	β (degree)	Failure characteristics
PH3-118.18	0	triaxial cell		axial fractures, cracks
PH3-118.32	2	triaxial cell		axial fractures, cracks
PH3-118.55	4	triaxial cell		axial fractures, cracks
PH3-118.69	6	triaxial cell	18	conjugate fractures, wedge-shaped ends
PH3-120.03	8	triaxial cell	22	shear fracture, splays
PH3-124.06	10	triaxial cell	23	shear fracture
PH3-124.20	15	triaxial cell	24	conjugate fractures, splays
PH3-124.34	20	triaxial cell	26	conjugate fractures, cracks
PH3-124.47	30	triaxial cell	25	shear fracture
PH3-124.61	40	triaxial cell	28	shear fracture
PH3-124.75	50	triaxial cell	25	shear fracture, splays
PH3-124.89	60	triaxial cell	25	shear fracture

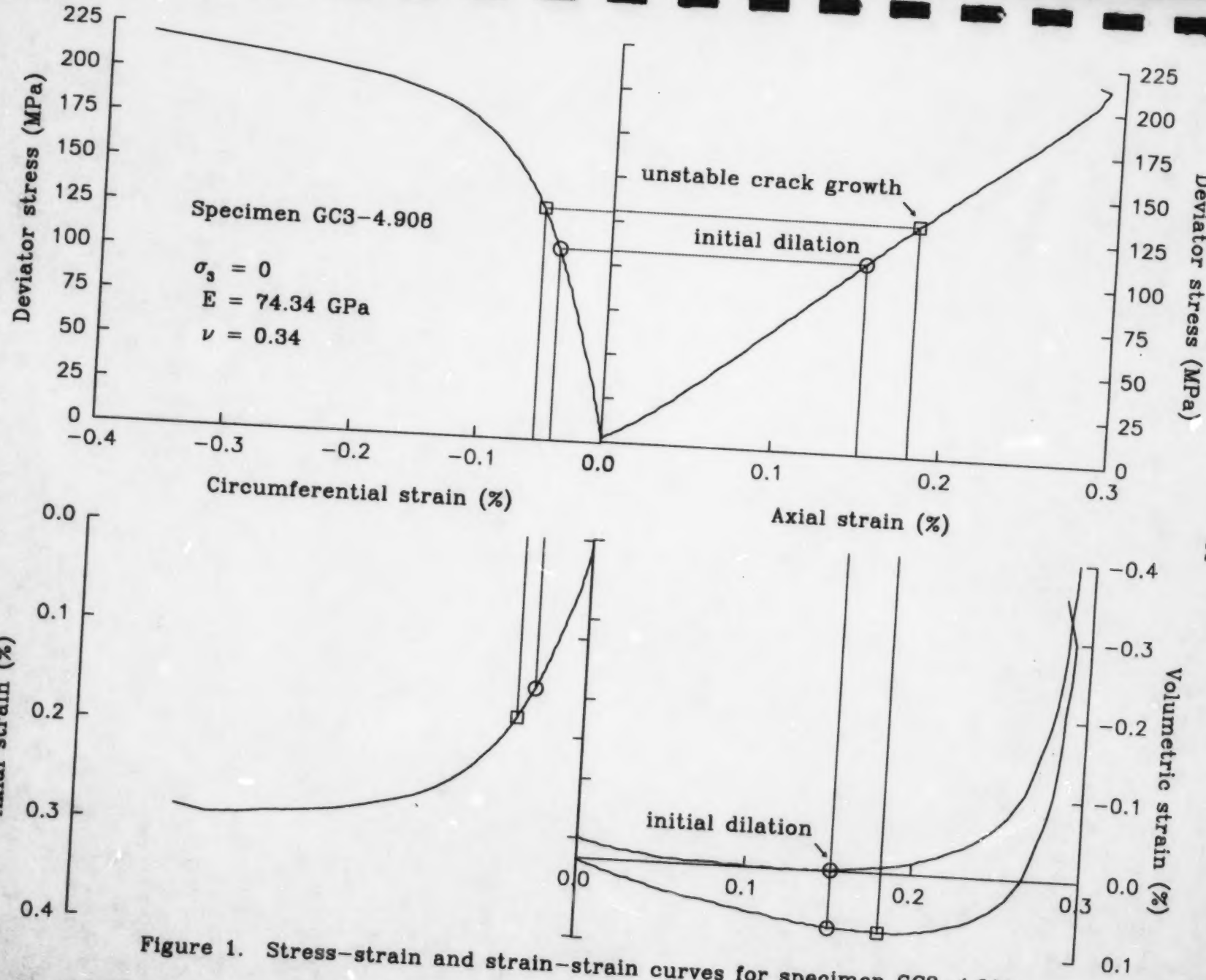

Figure 1. Stress–strain and strain–strain curves for specimen GC3–4.908.

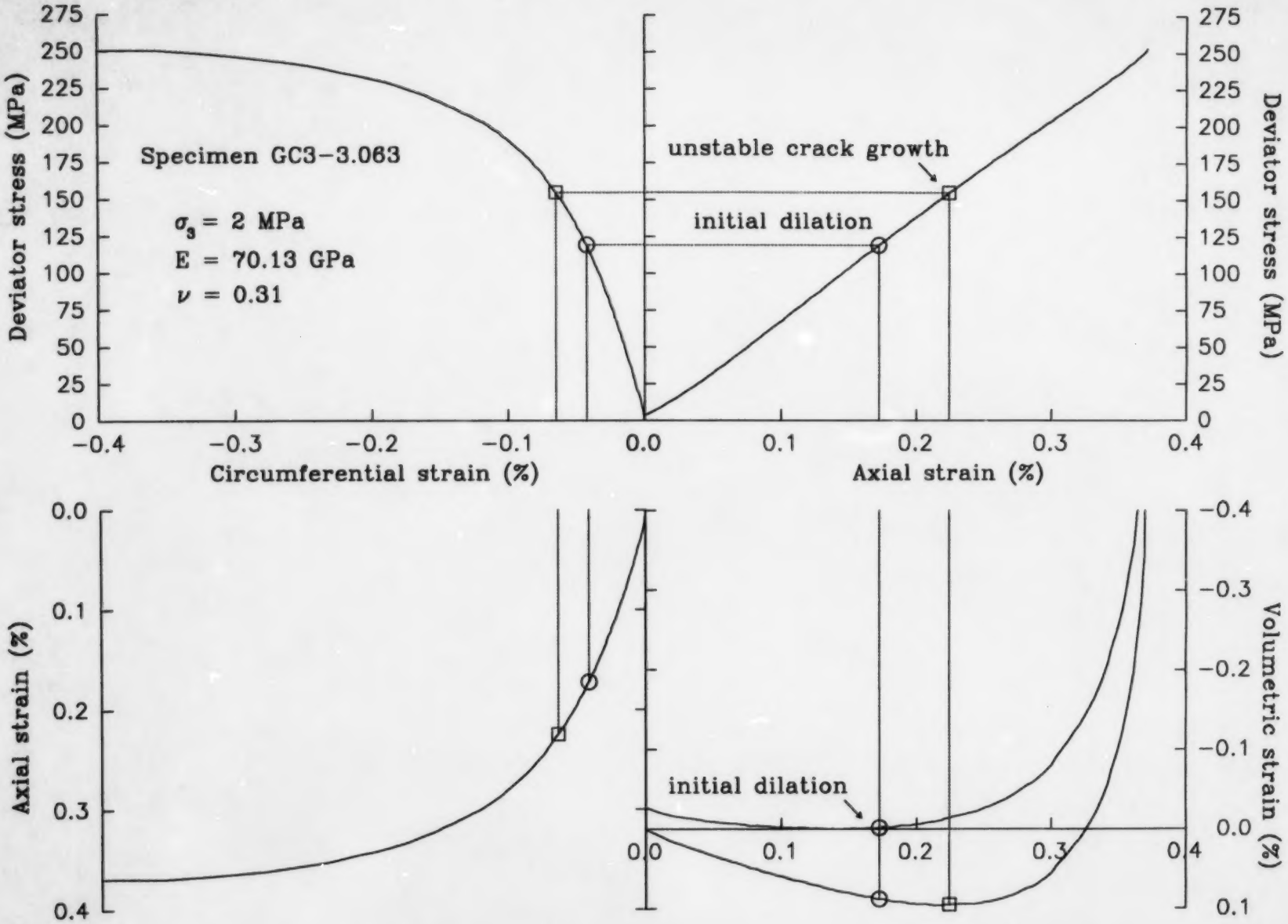

Figure 2. Stress–strain and strain–strain curves for specimen GC3–3.063.

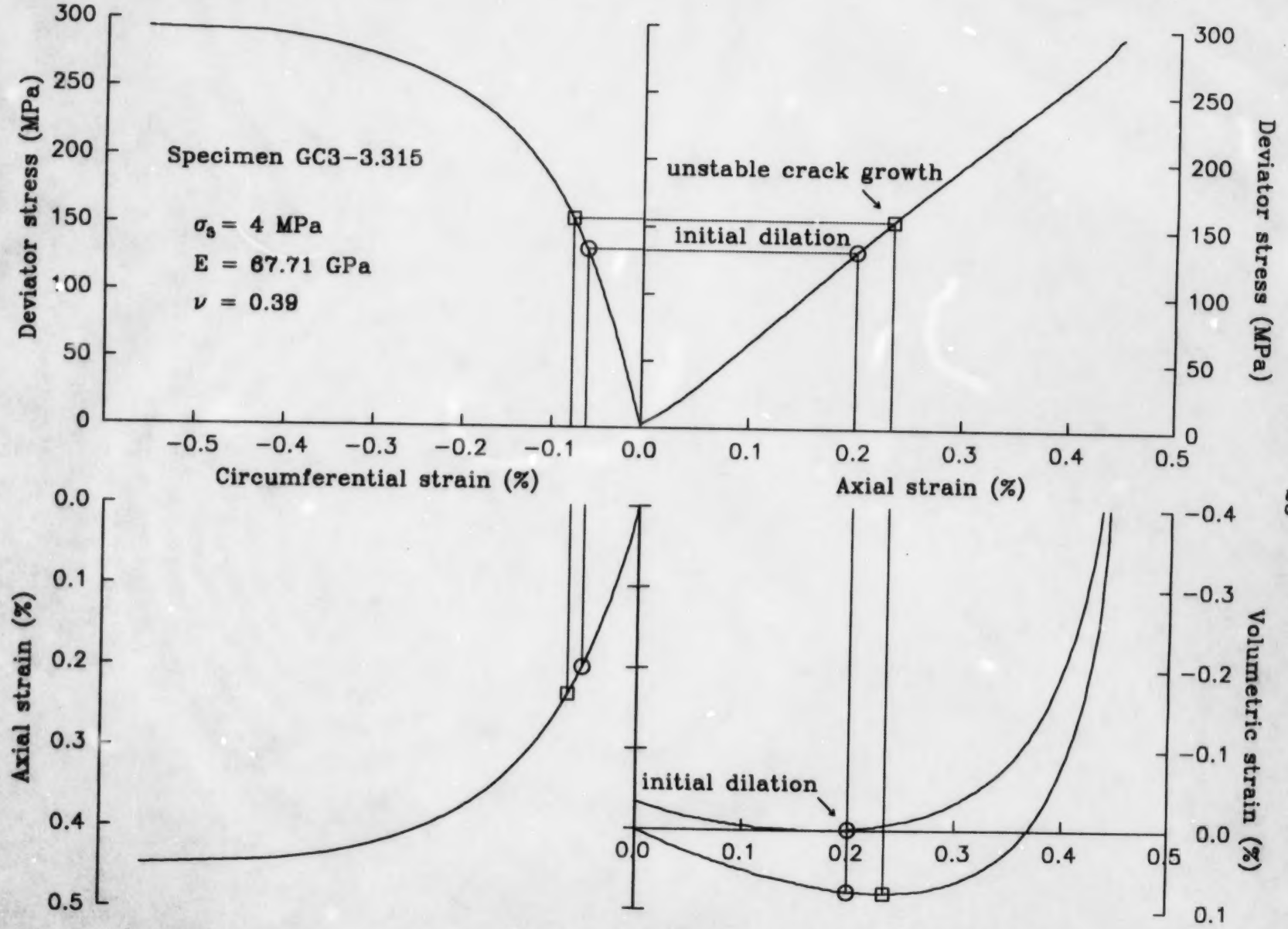

Figure 3. Stress–strain and strain–strain curves for specimen GC3–3.315.

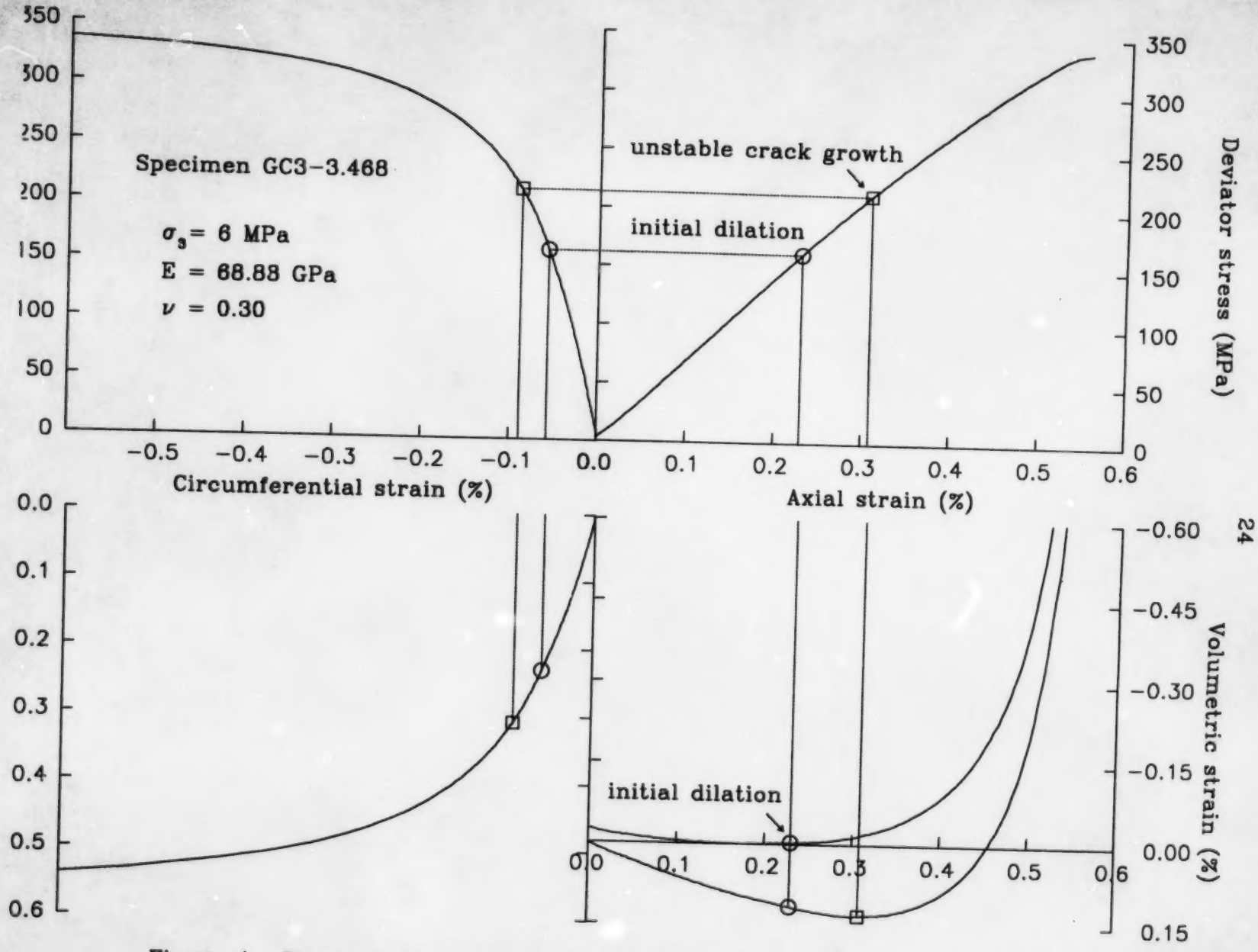

Figure 4. Stress–strain and strain–strain curves for specimen GC3–3.468.

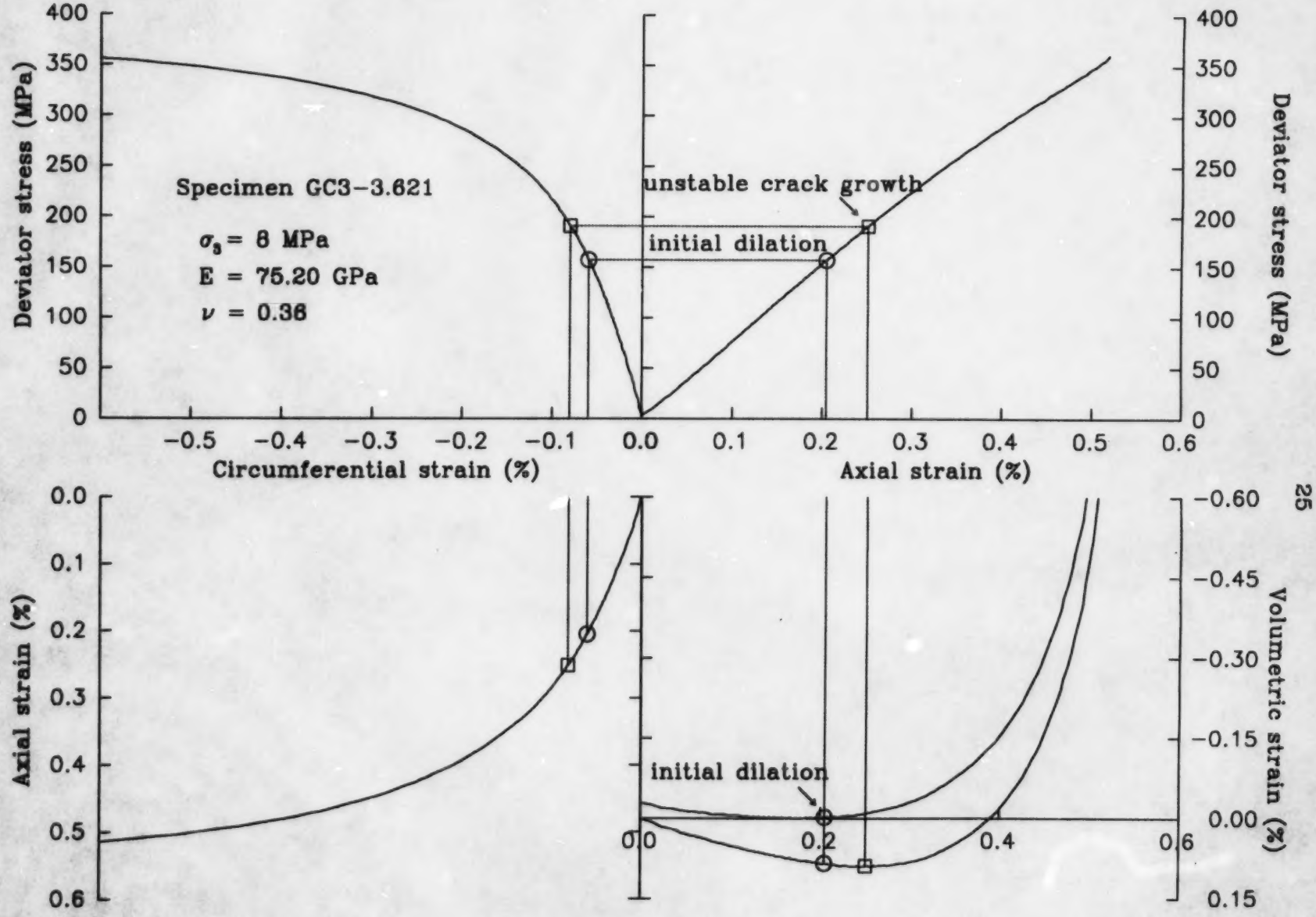

Figure 5. Stress–strain and strain–strain curves for specimen GC3–3.621.

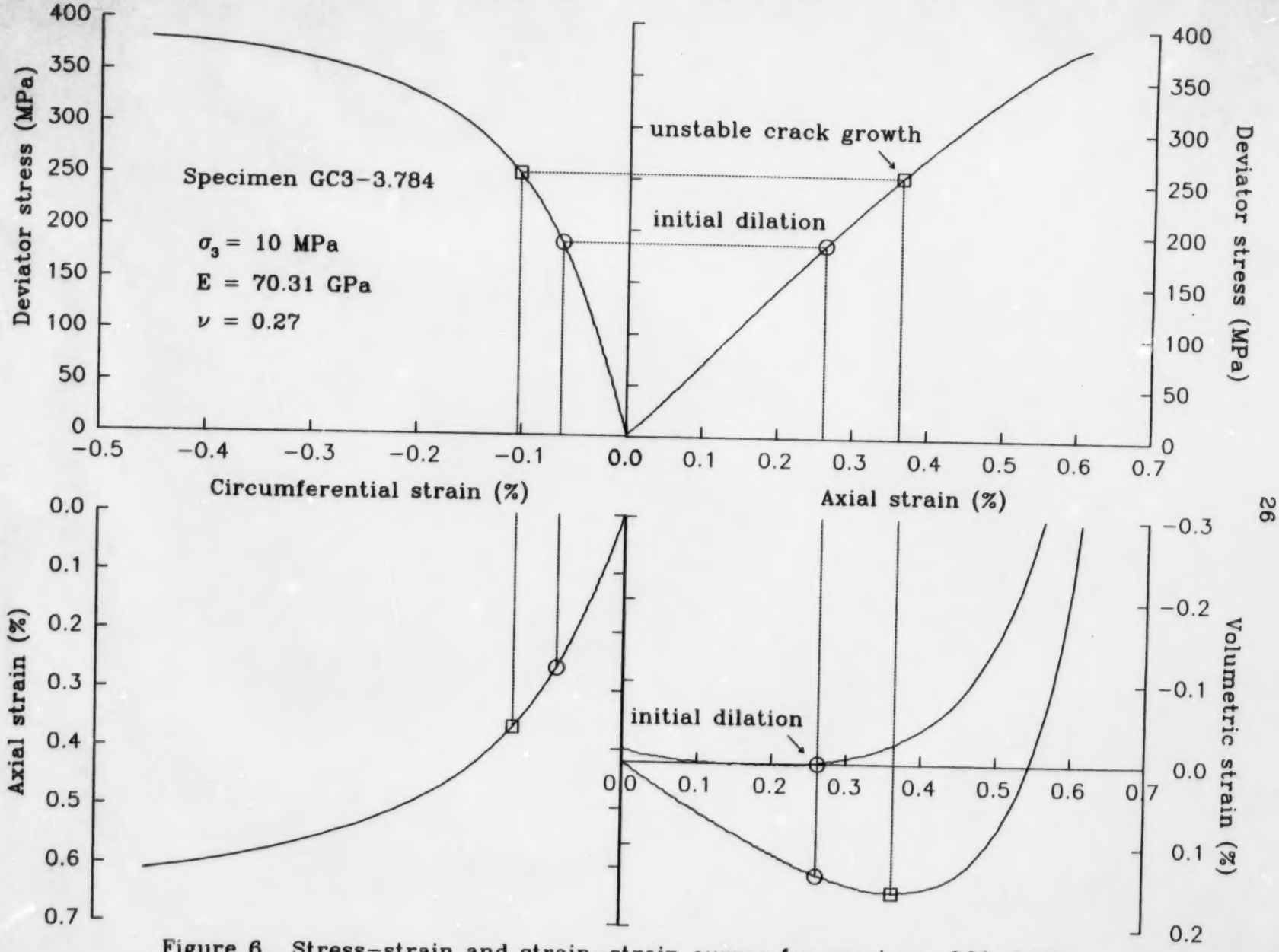

Figure 6. Stress–strain and strain–strain curves for specimen GC3–3.784.

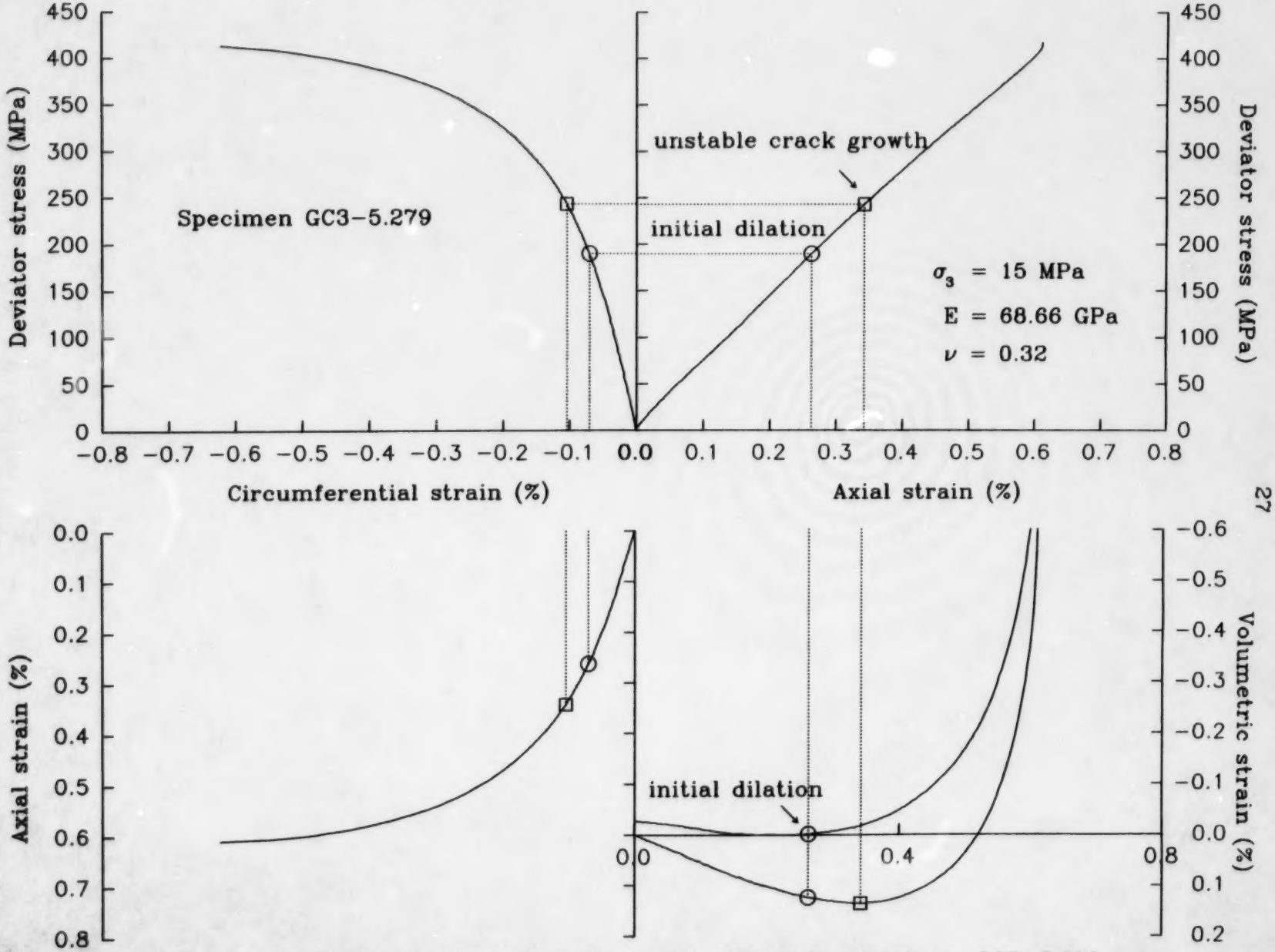

Figure 7. Stress–strain and strain–strain curves for specimen GC3–5.279.

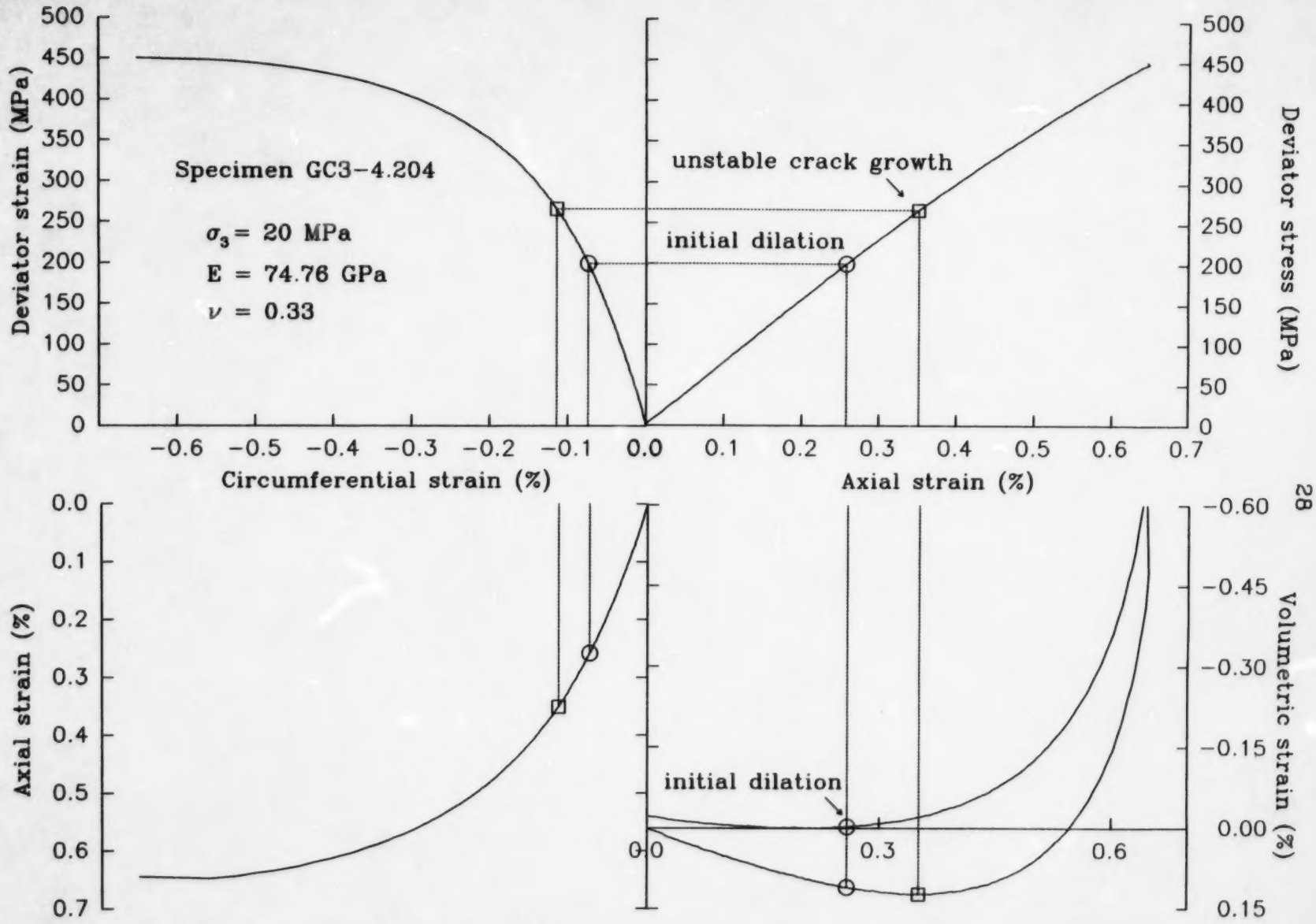

Figure 8. Stress–strain and strain–strain curves for specimen GC3-4.204.

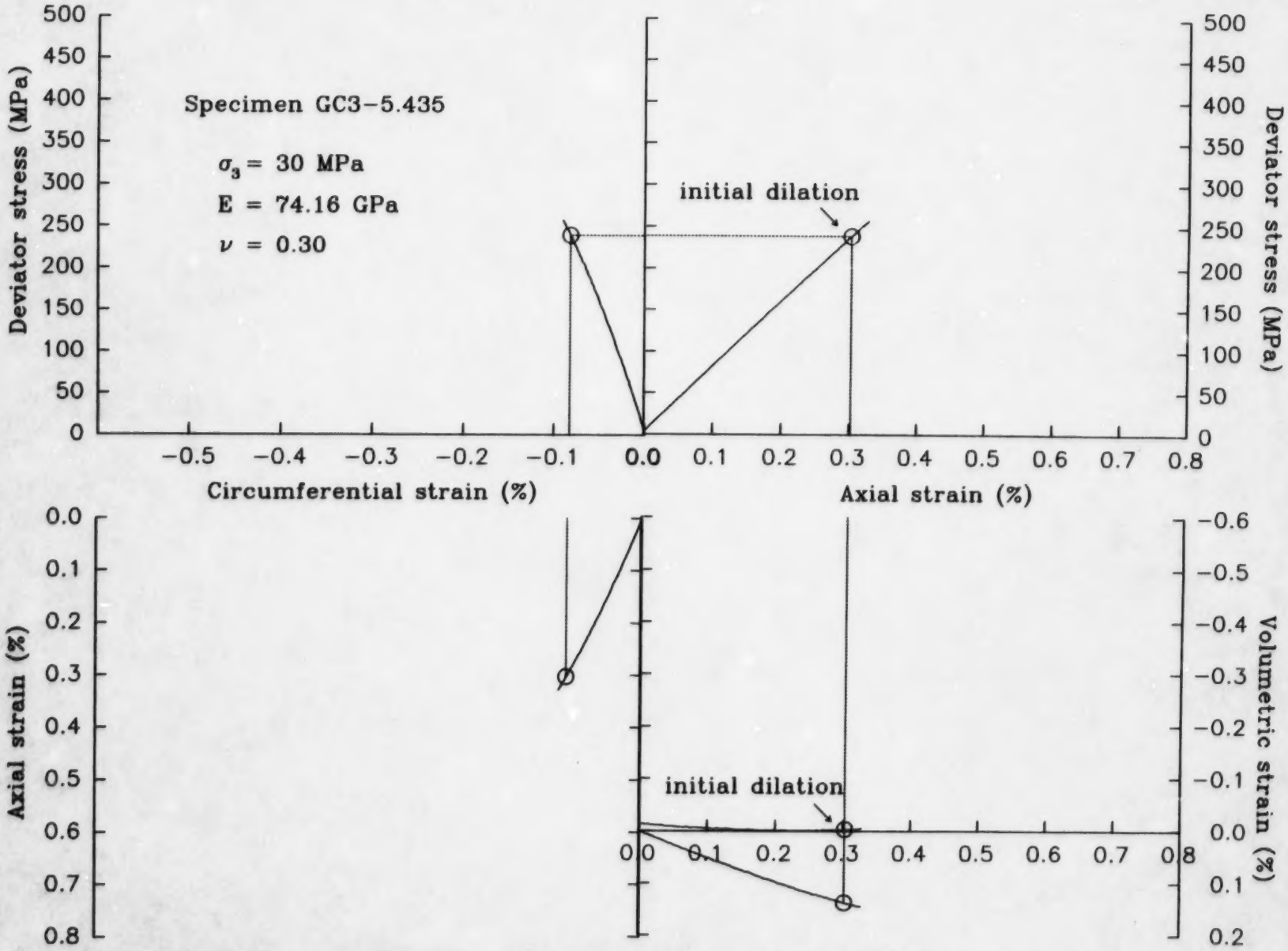

Figure 9. Stress–strain and strain–strain curves for specimen GC3-5.435.

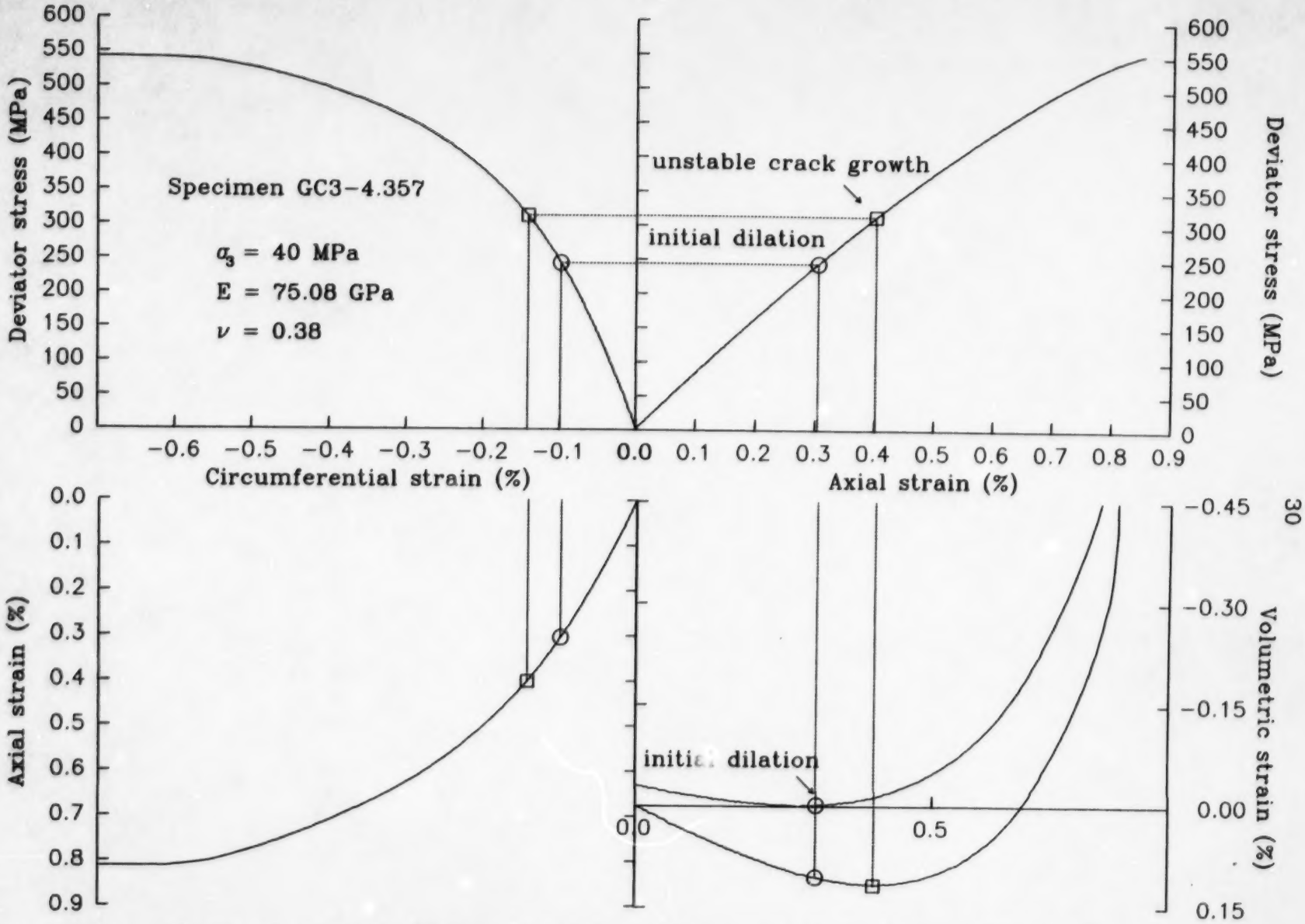

Figure 10. Stress–strain and strain–strain curves for specimen GC3–4.357.

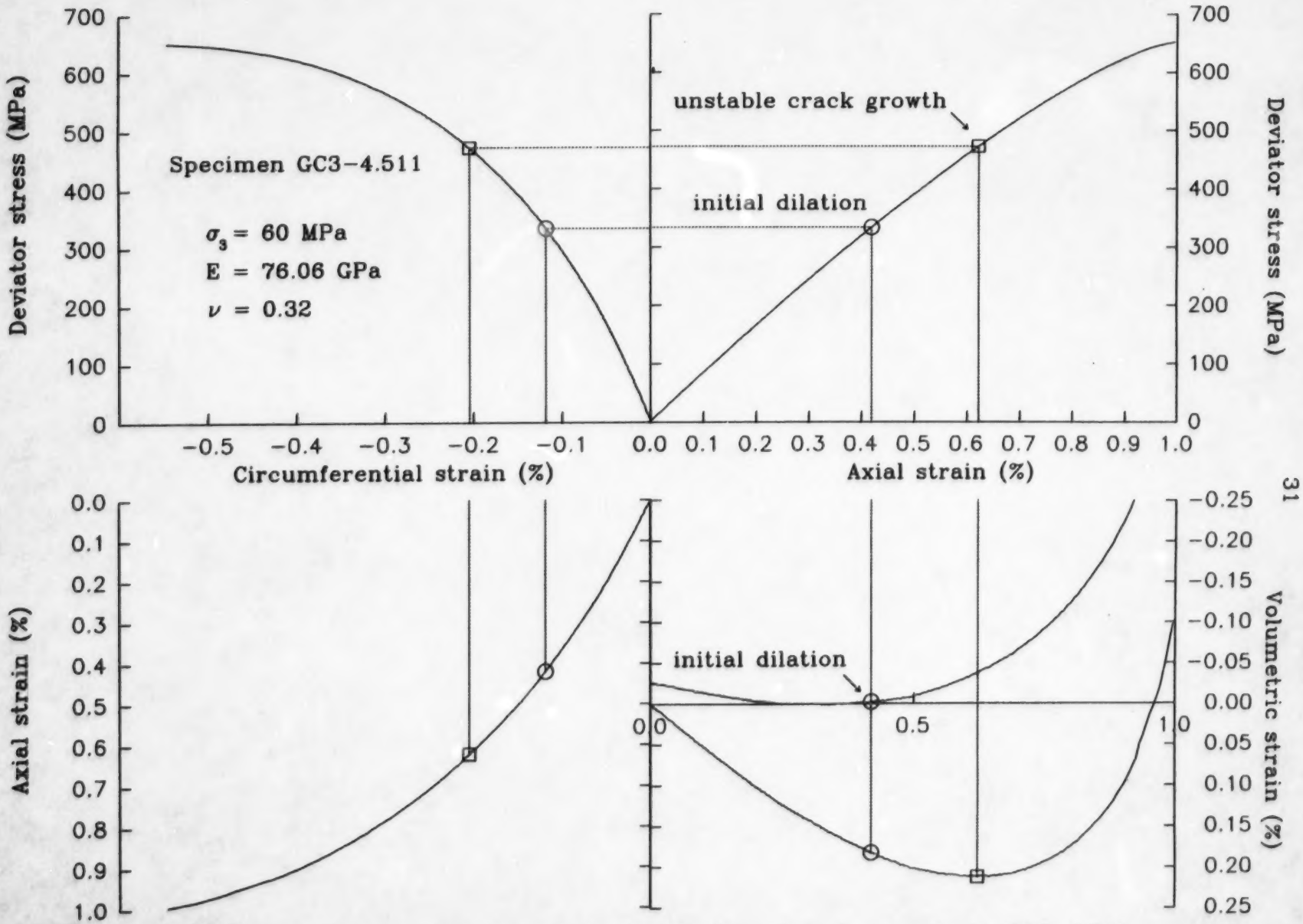

Figure 11. Stress–strain and strain–strain curves for specimen GC3–4.511.

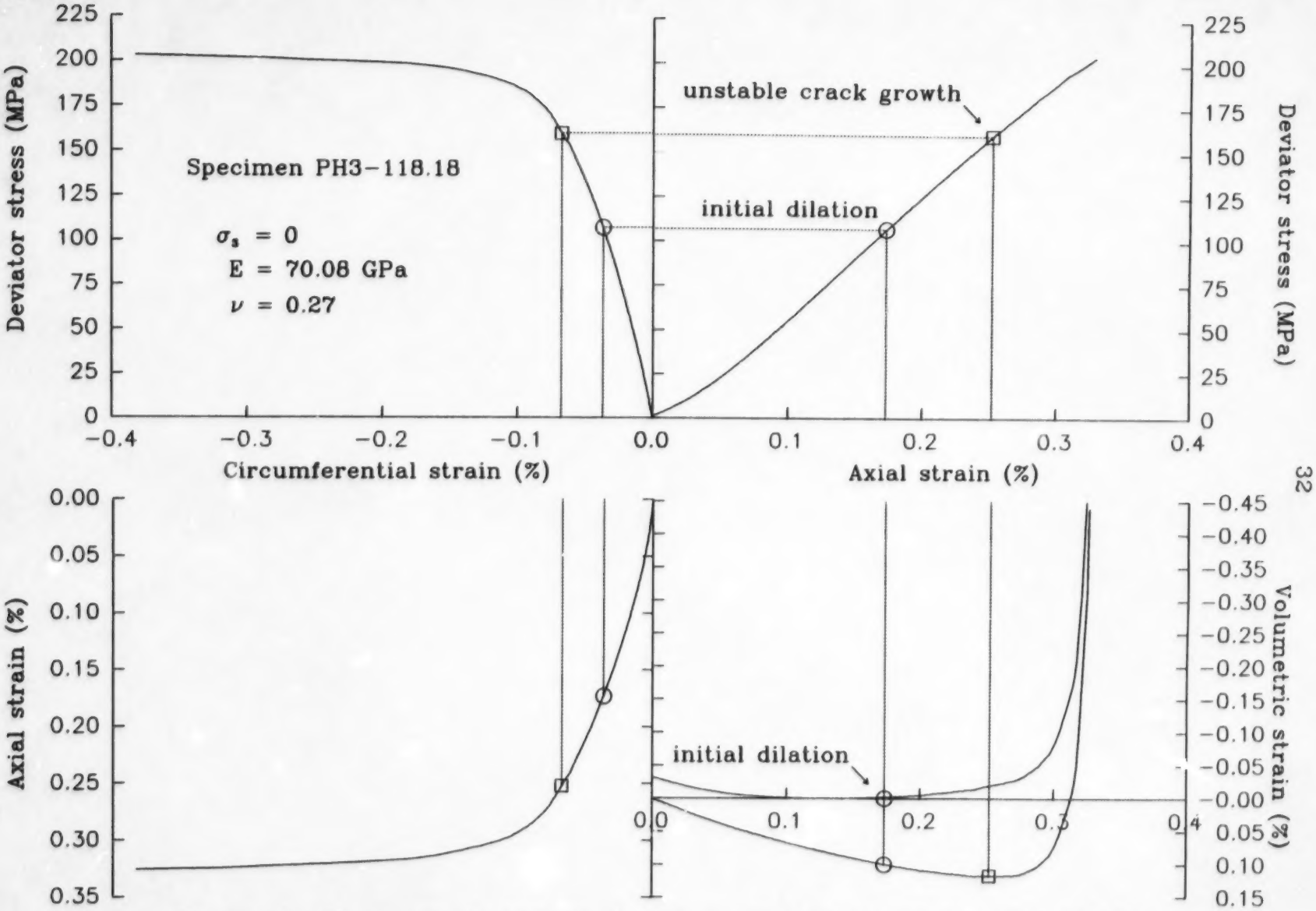

Figure 12. Stress–strain and strain–strain curves for specimen PH3–118.18.

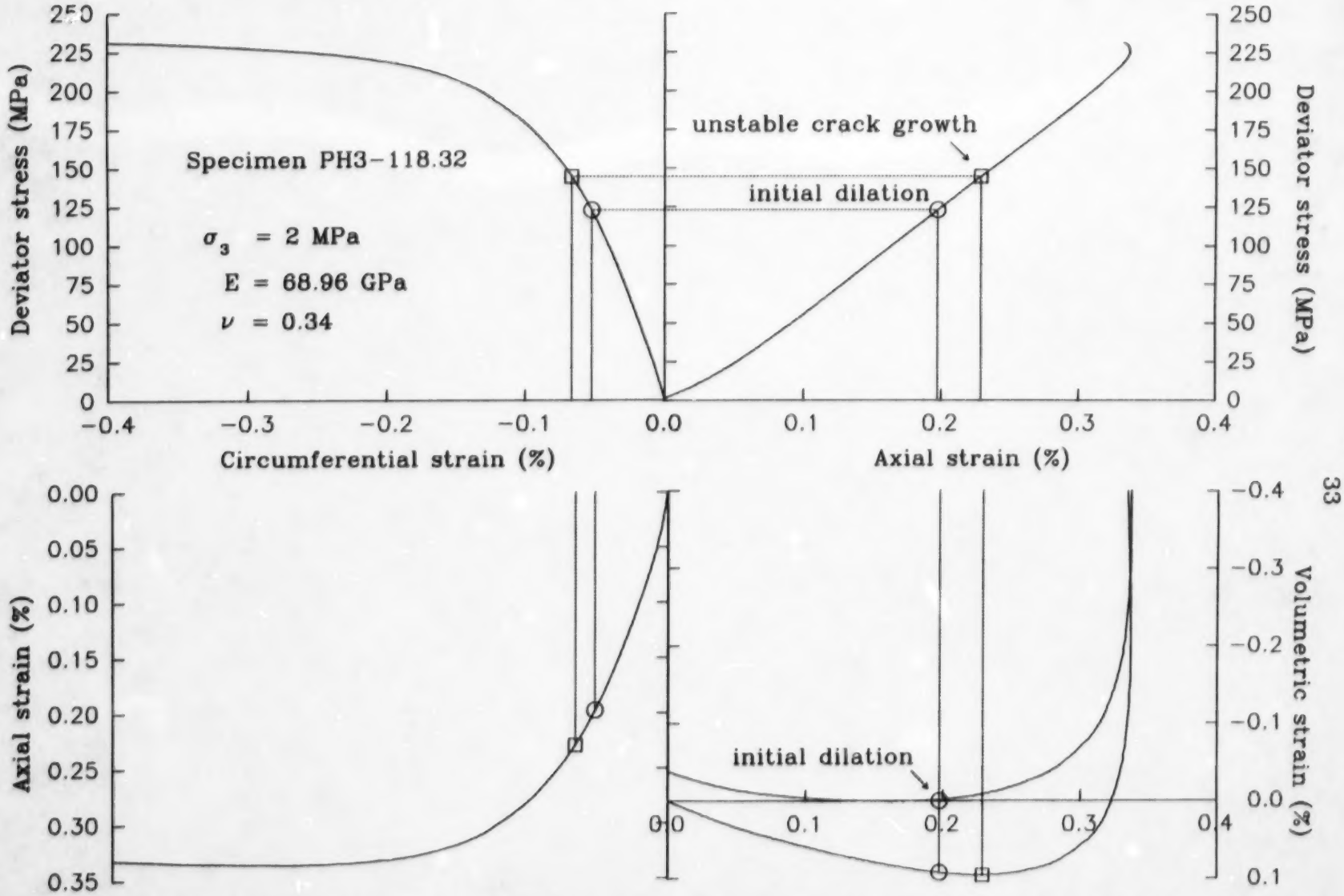

Figure 13. Stress-strain and strain-strain curves for specimen PH3-118.32.

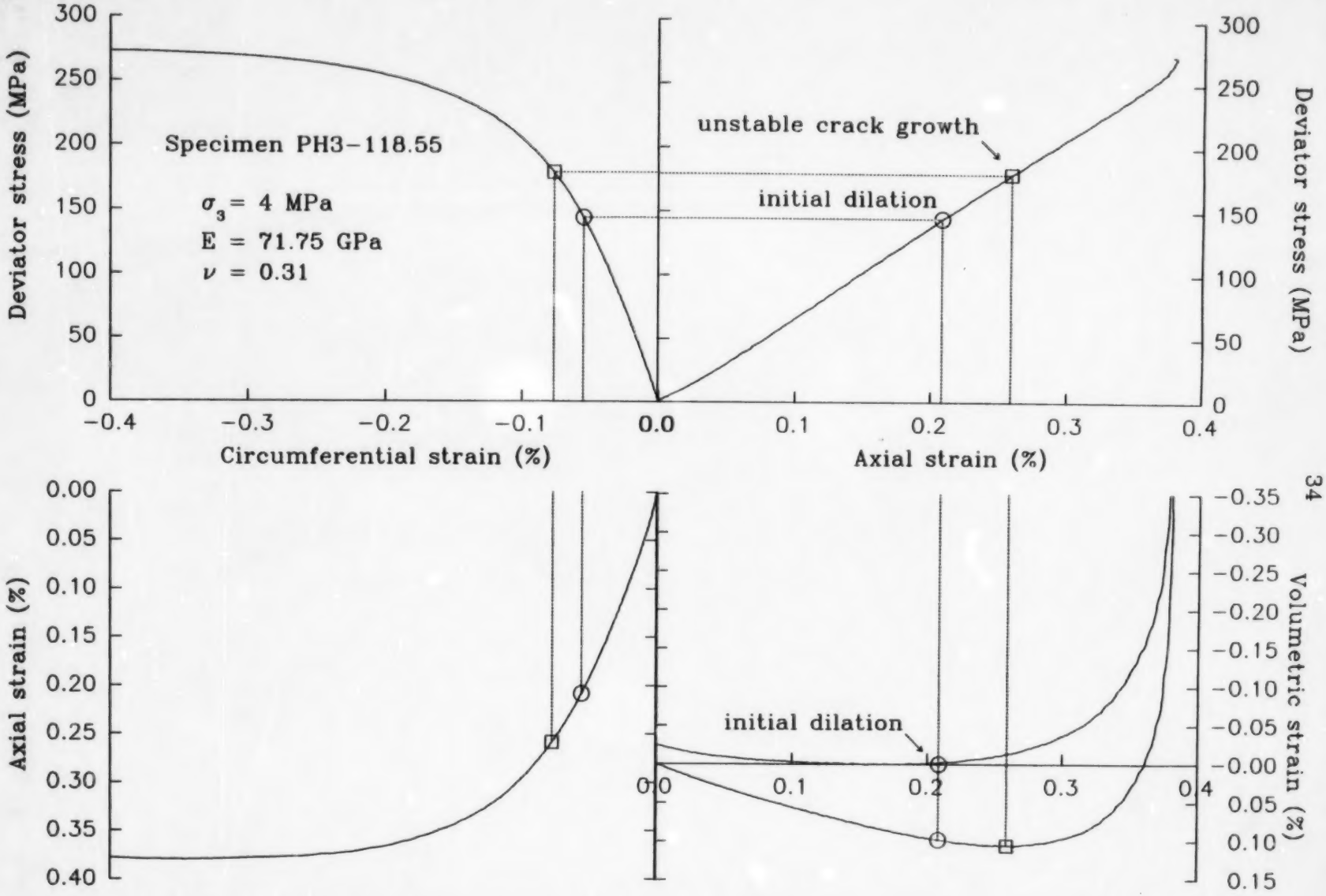

Figure 14. Stress–strain and strain–strain curves for specimen PH3–118.55.

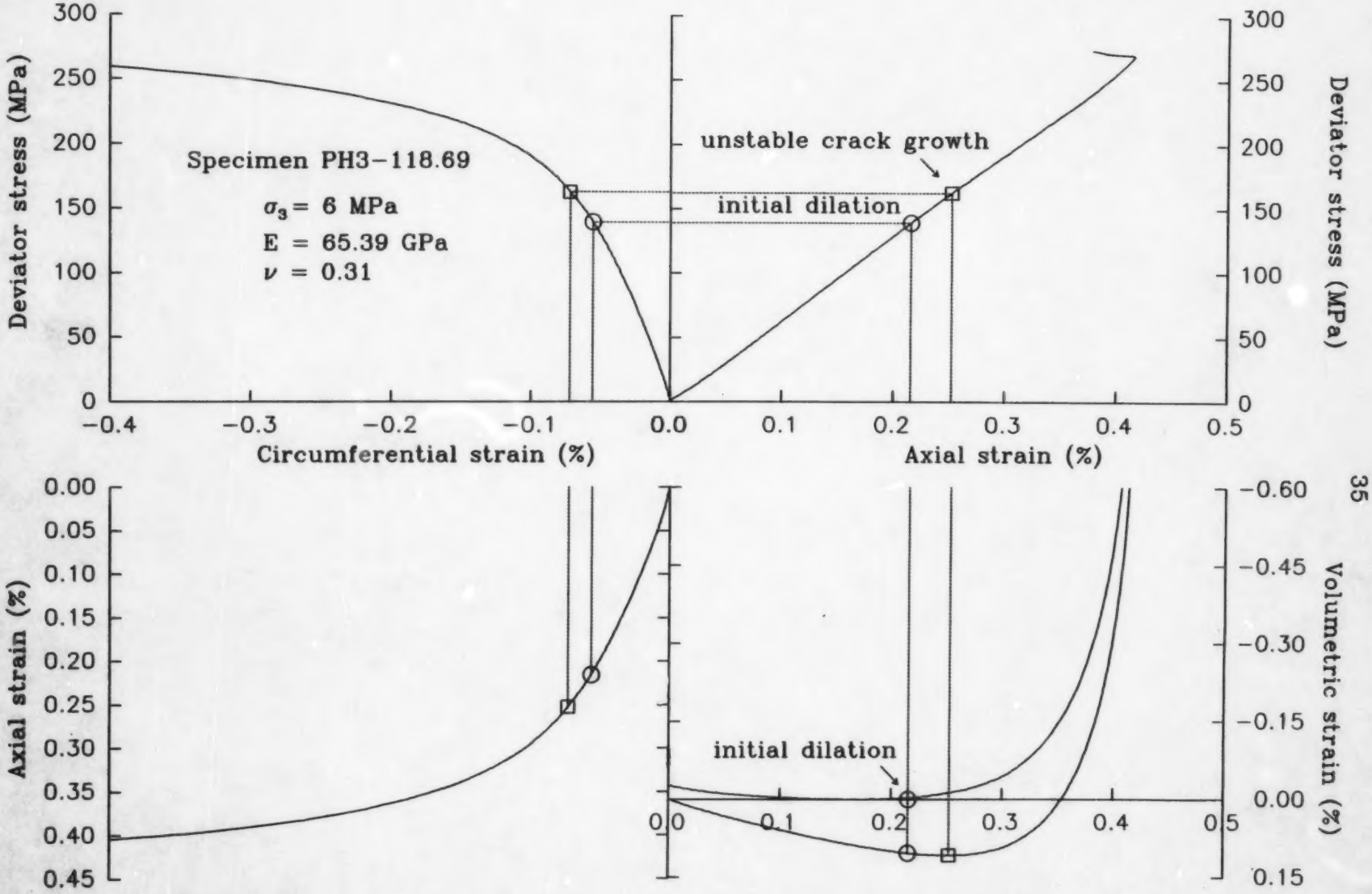

Figure 15. Stress–strain and strain–strain curves for specimen PH3–118.69.

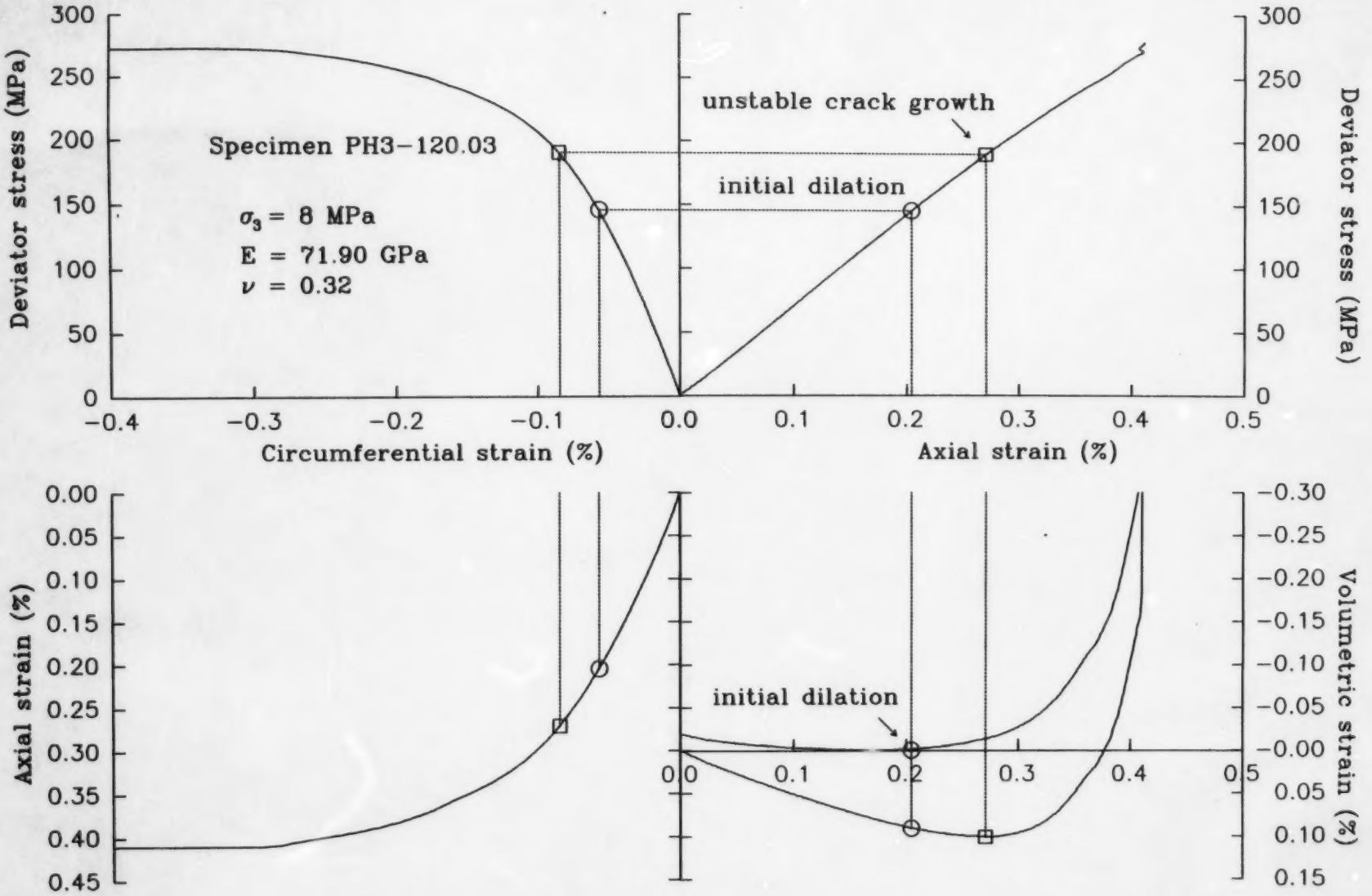

Figure 16. Stress-strain and strain-strain curves for specimen PH3-120.03.

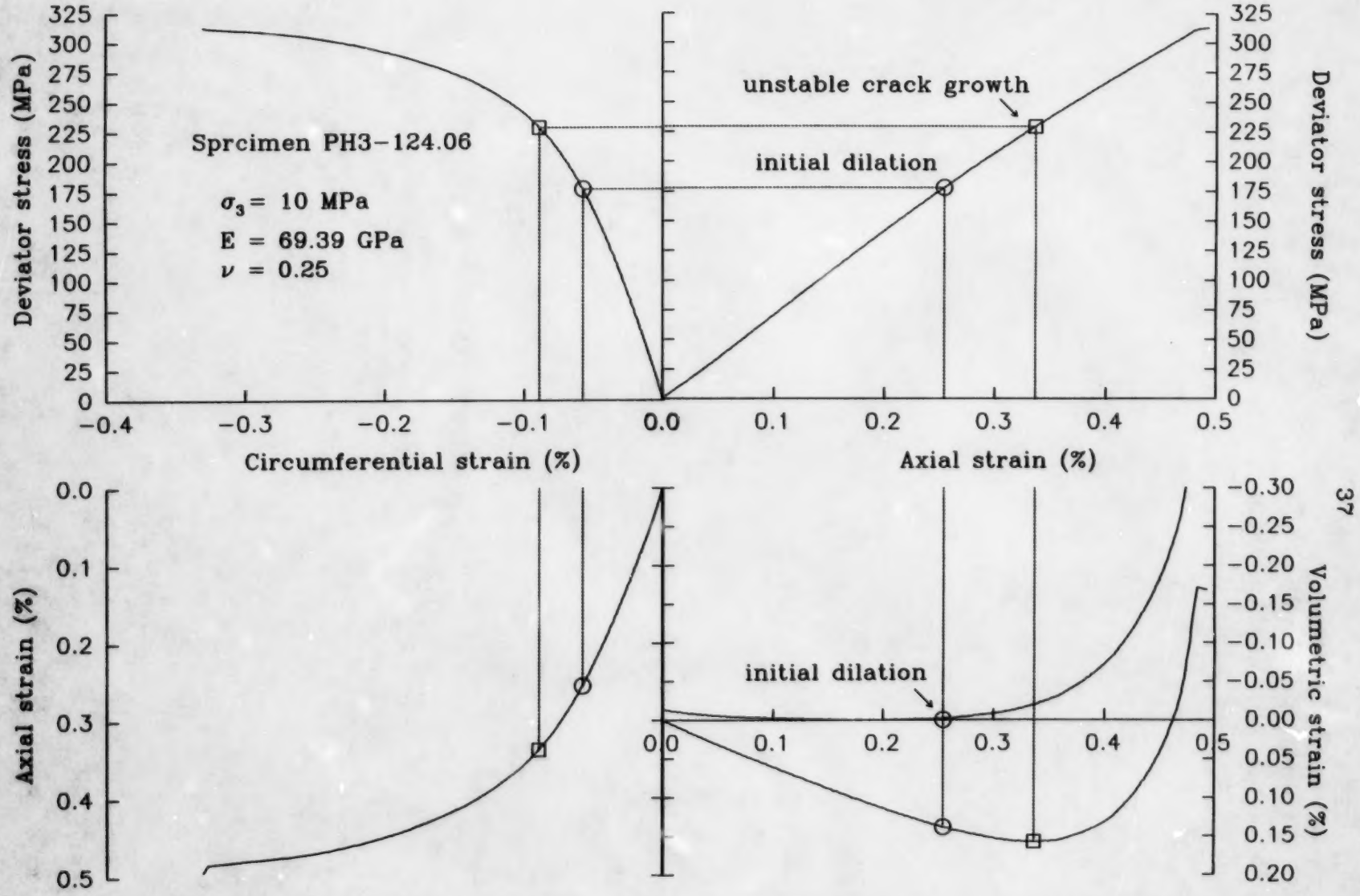

Figure 17. Stress–strain and strain–strain curves for specimen PH3–124.06.

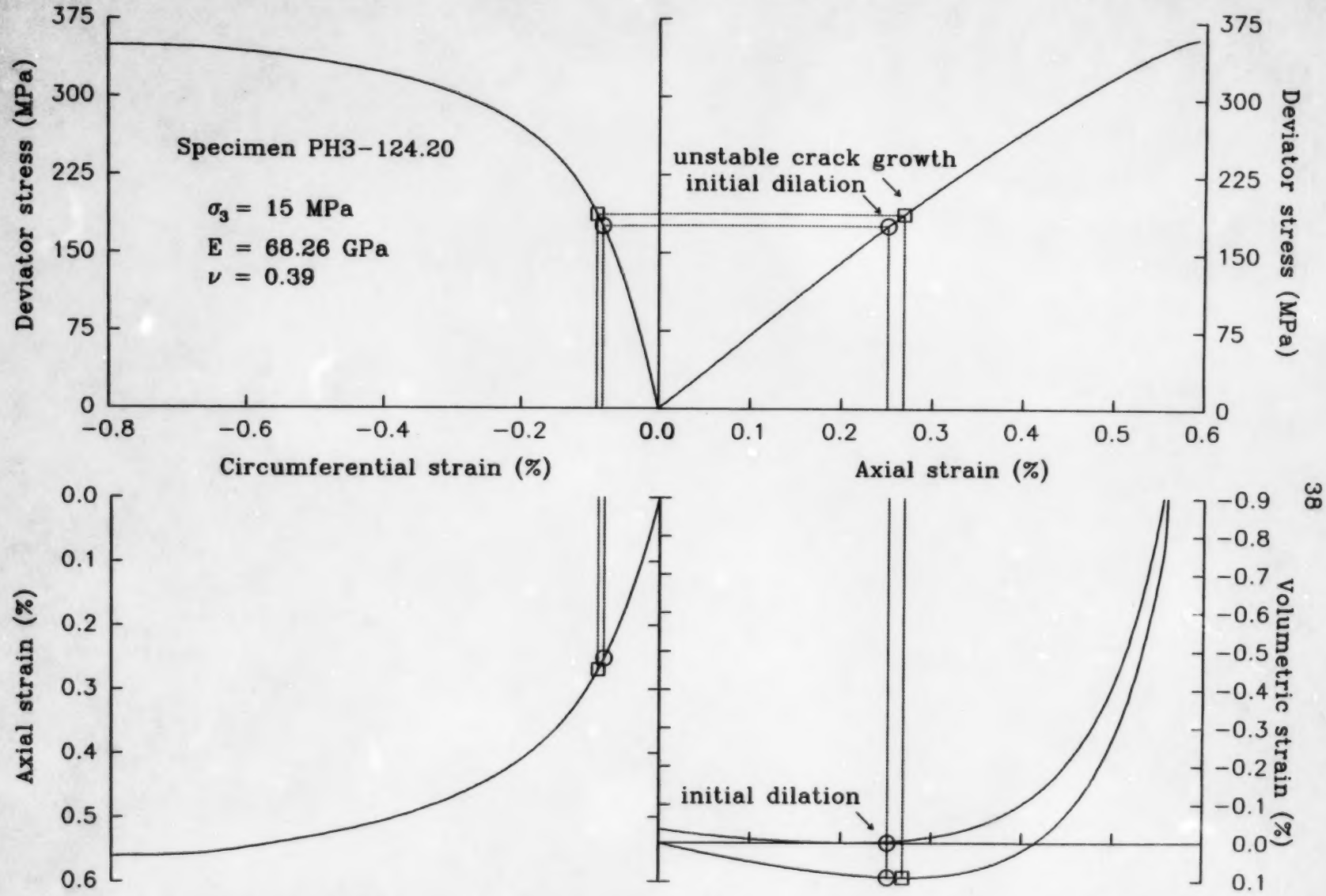

Figure 18. Stress–strain and strain–strain curves for specimen PH3–124.20.

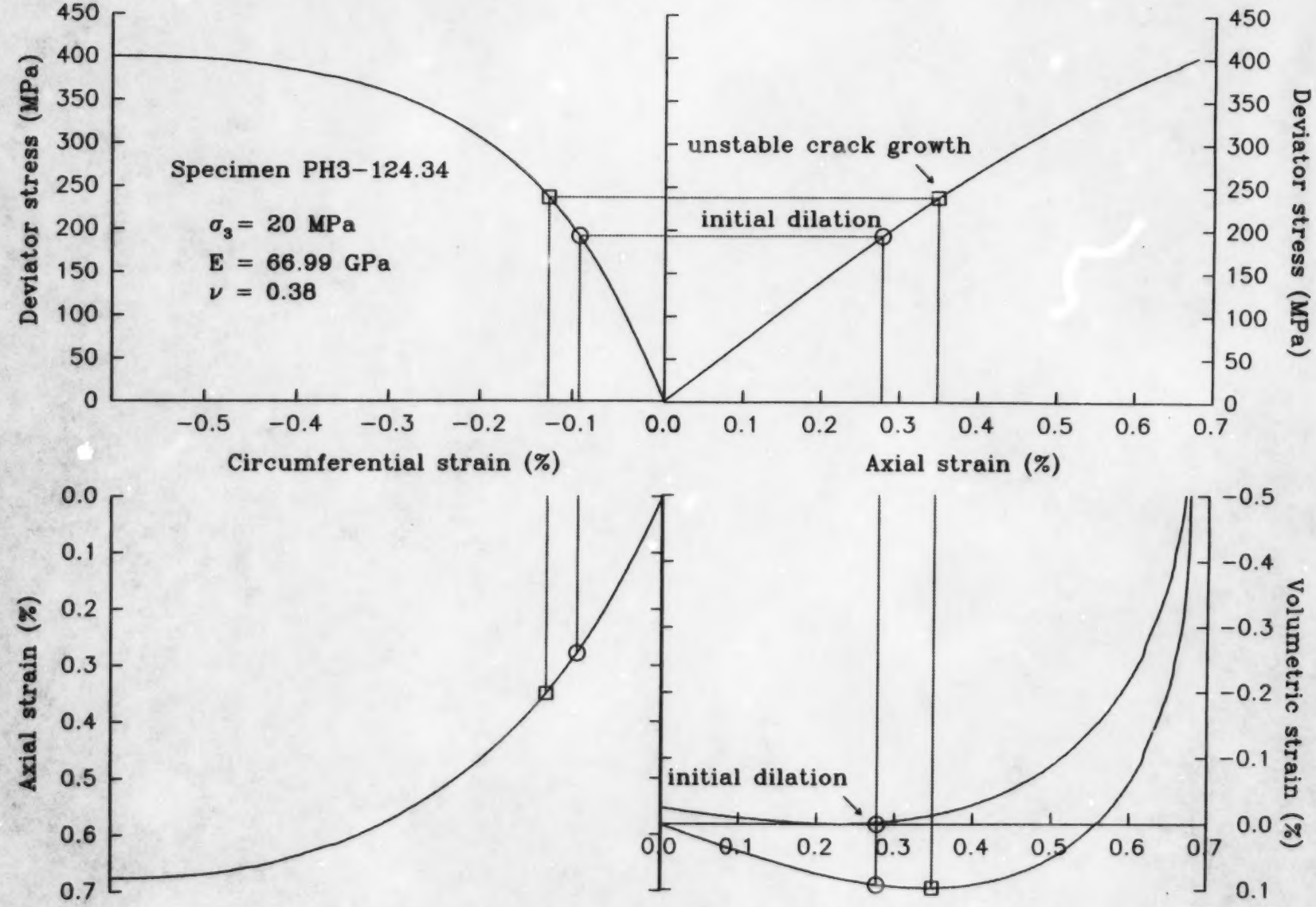

Figure 19. Stress–strain and strain–strain curves for specimen PH3–124.34.

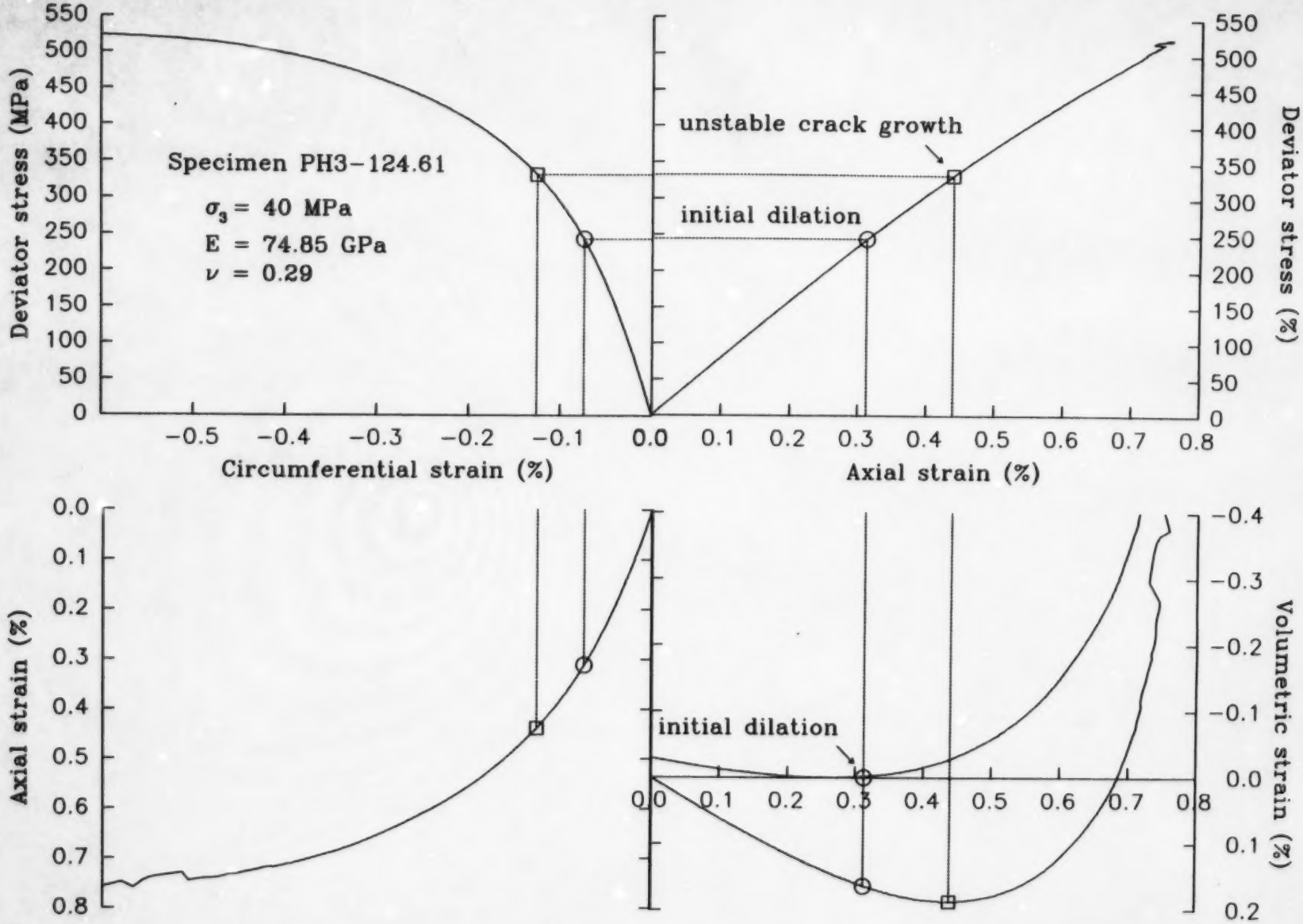

Figure 20. Stress–strain and strain–strain curves for specimen PH3–124.61.

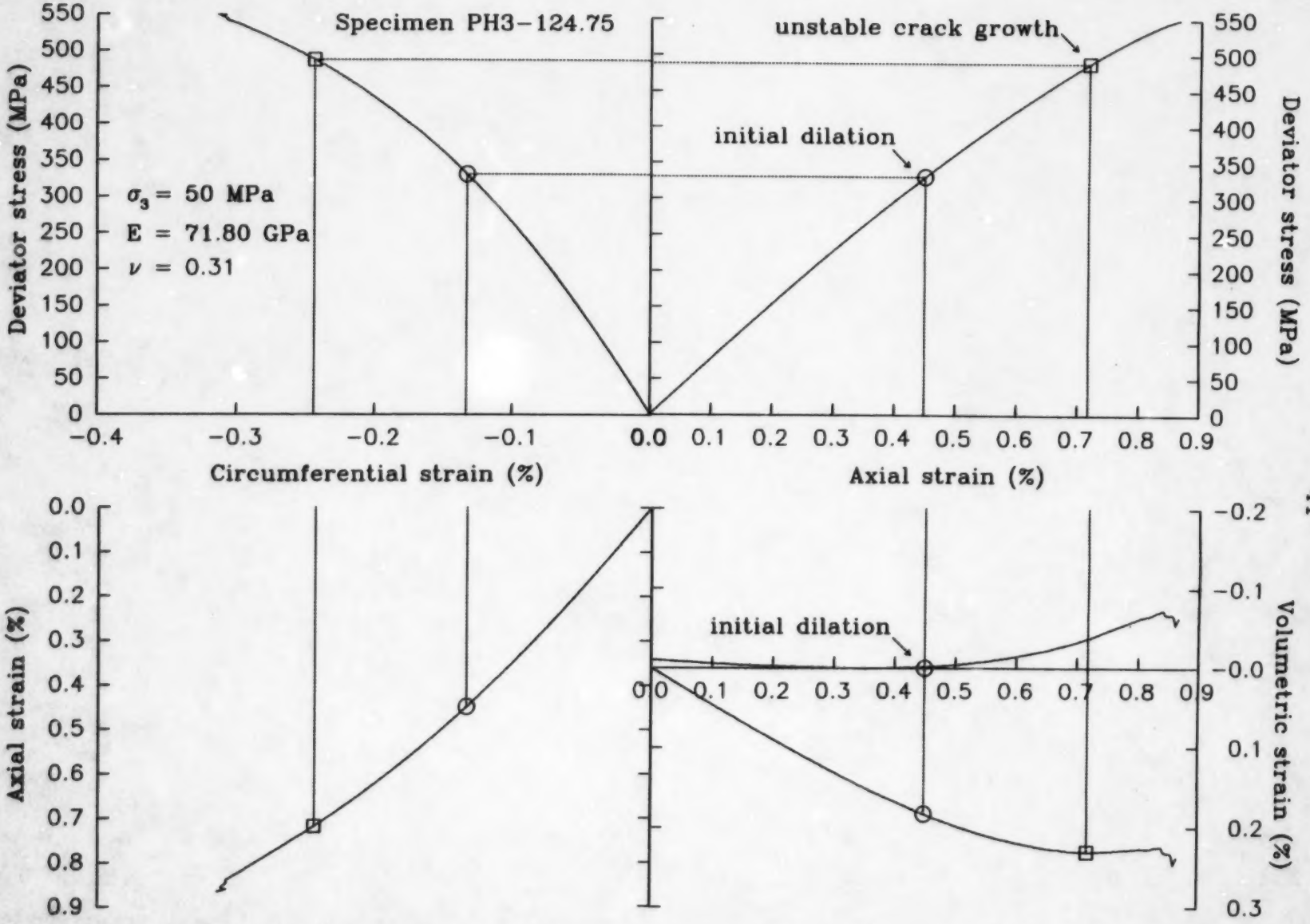

Figure 21. Stress–strain and strain–strain curves for specimen PH3–124.75.

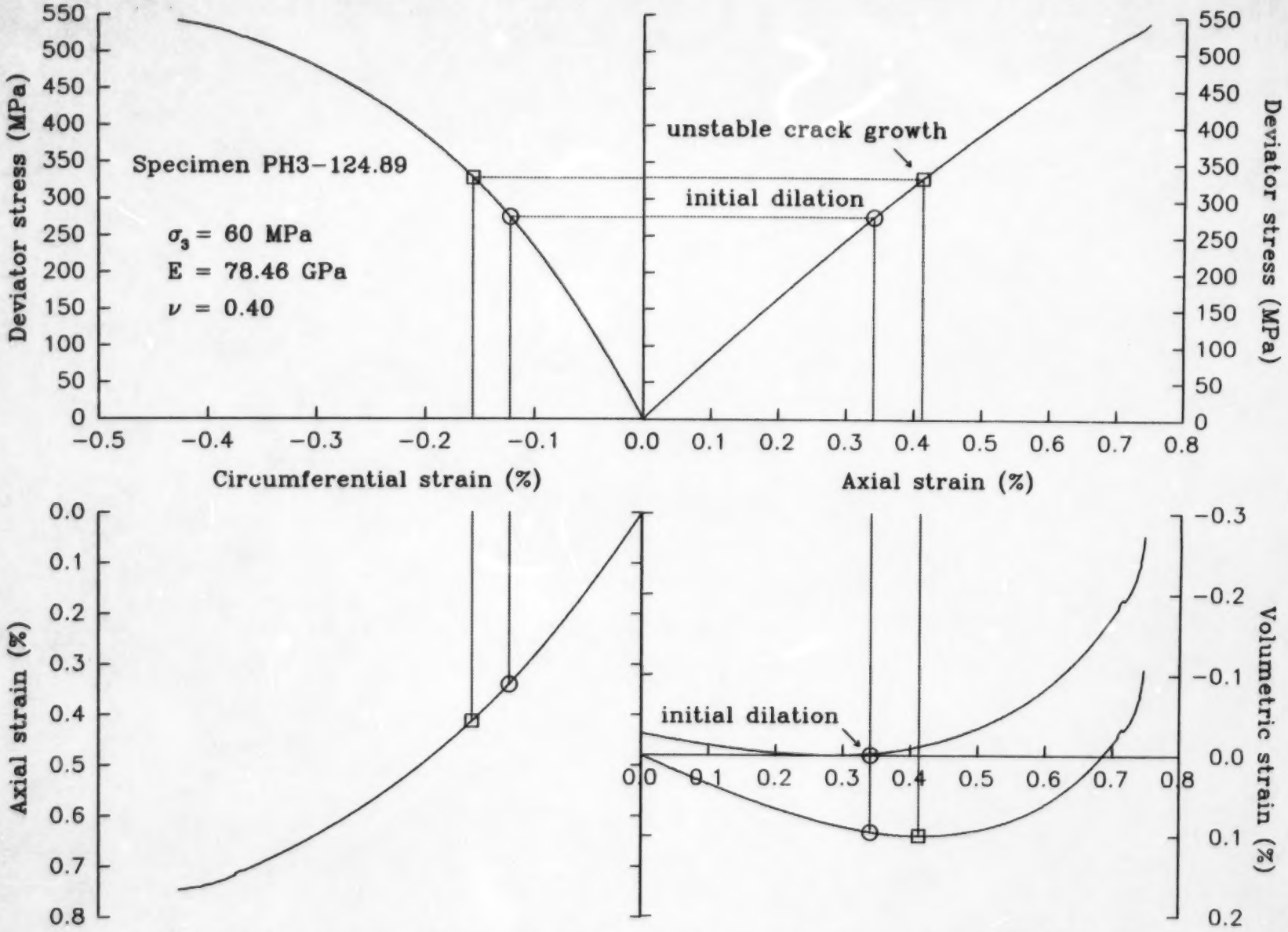

Figure 22. Stress–strain and strain–strain curves for specimen PH3–124.89.

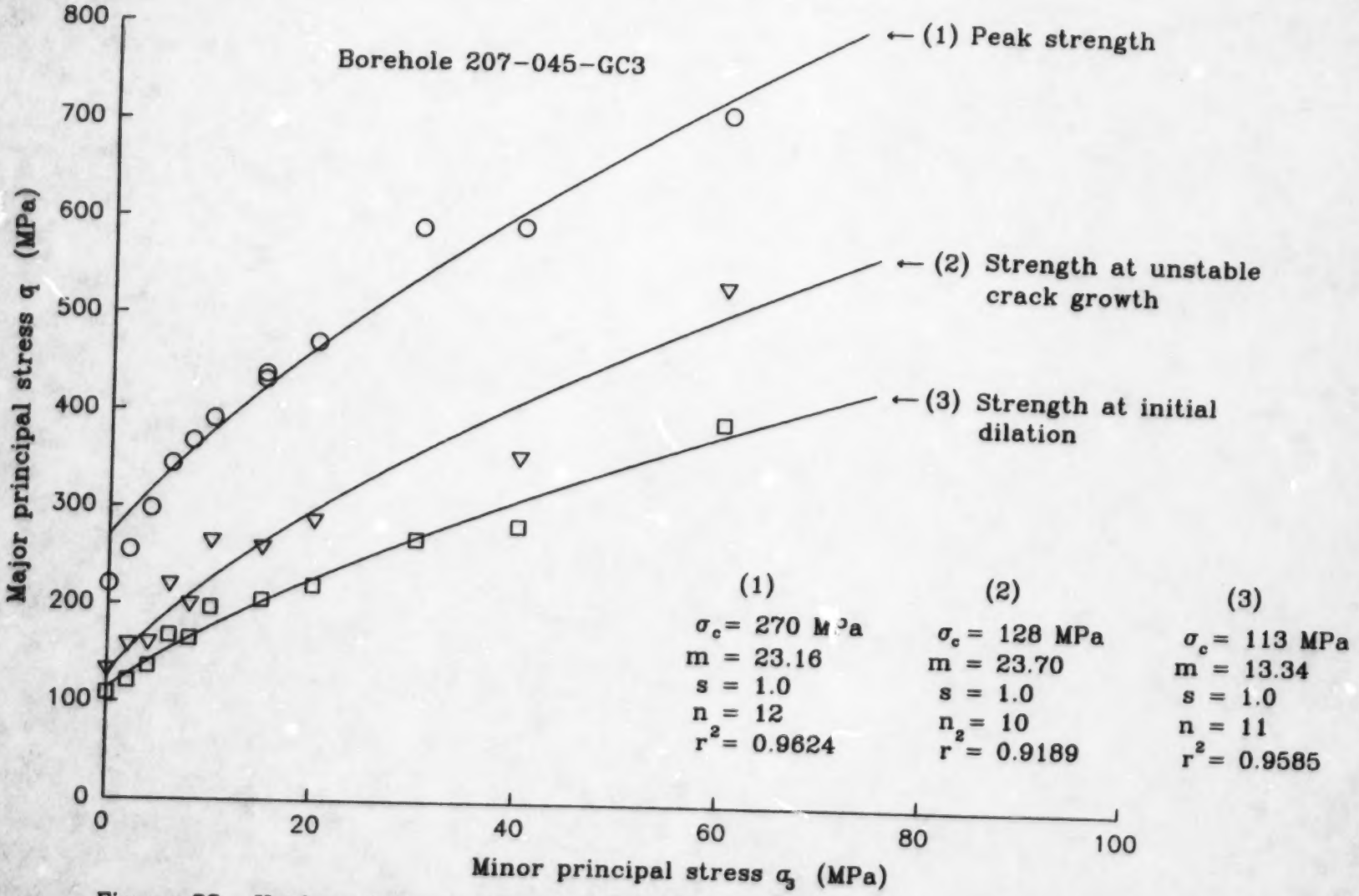

Figure 23. Hoek and Brown failure envelopes for specimens from borehole 207-045-GC3.

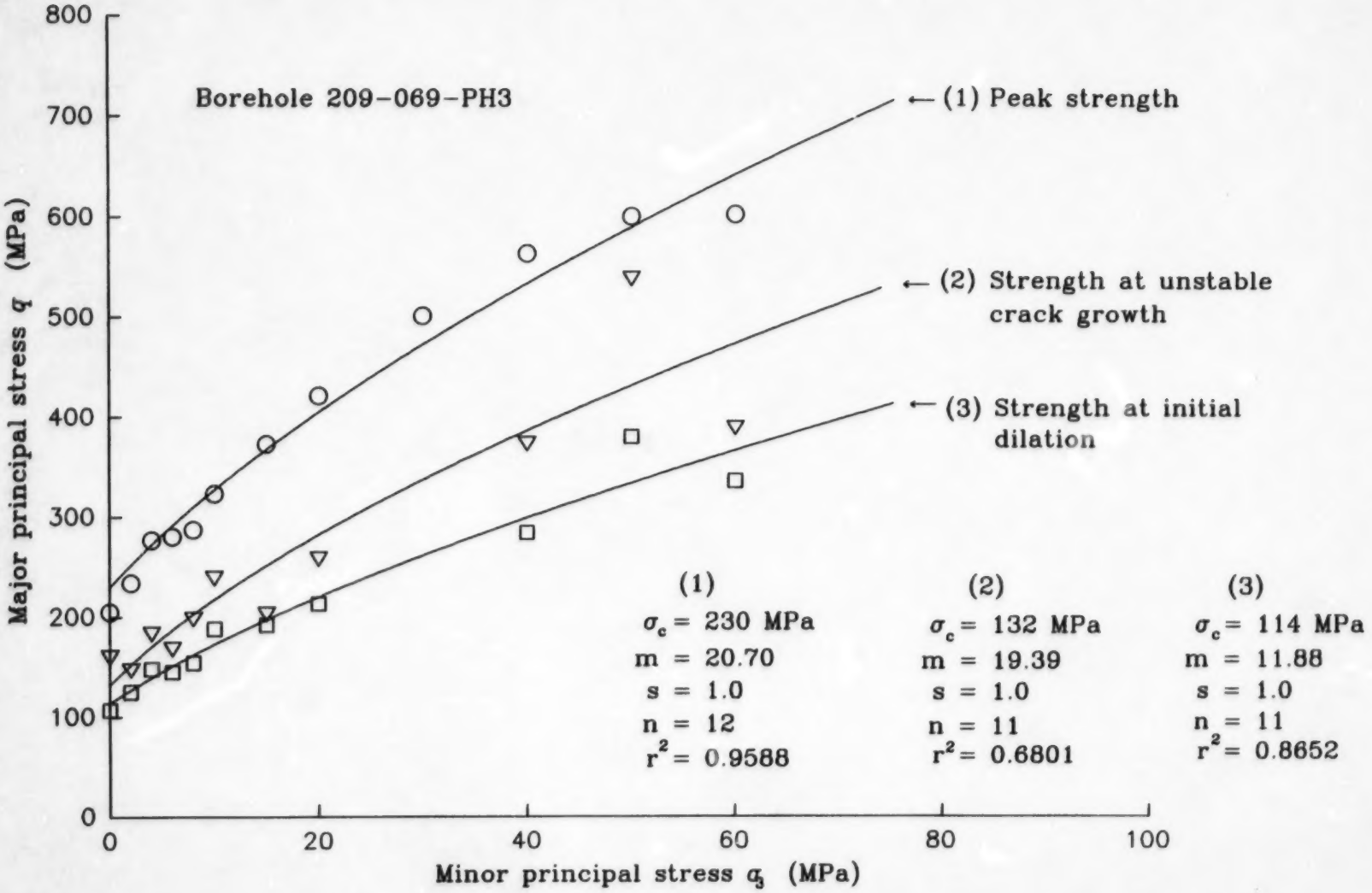

Figure 24. Hoek and Brown failure envelopes for specimens from borehole 209-069-PH3.

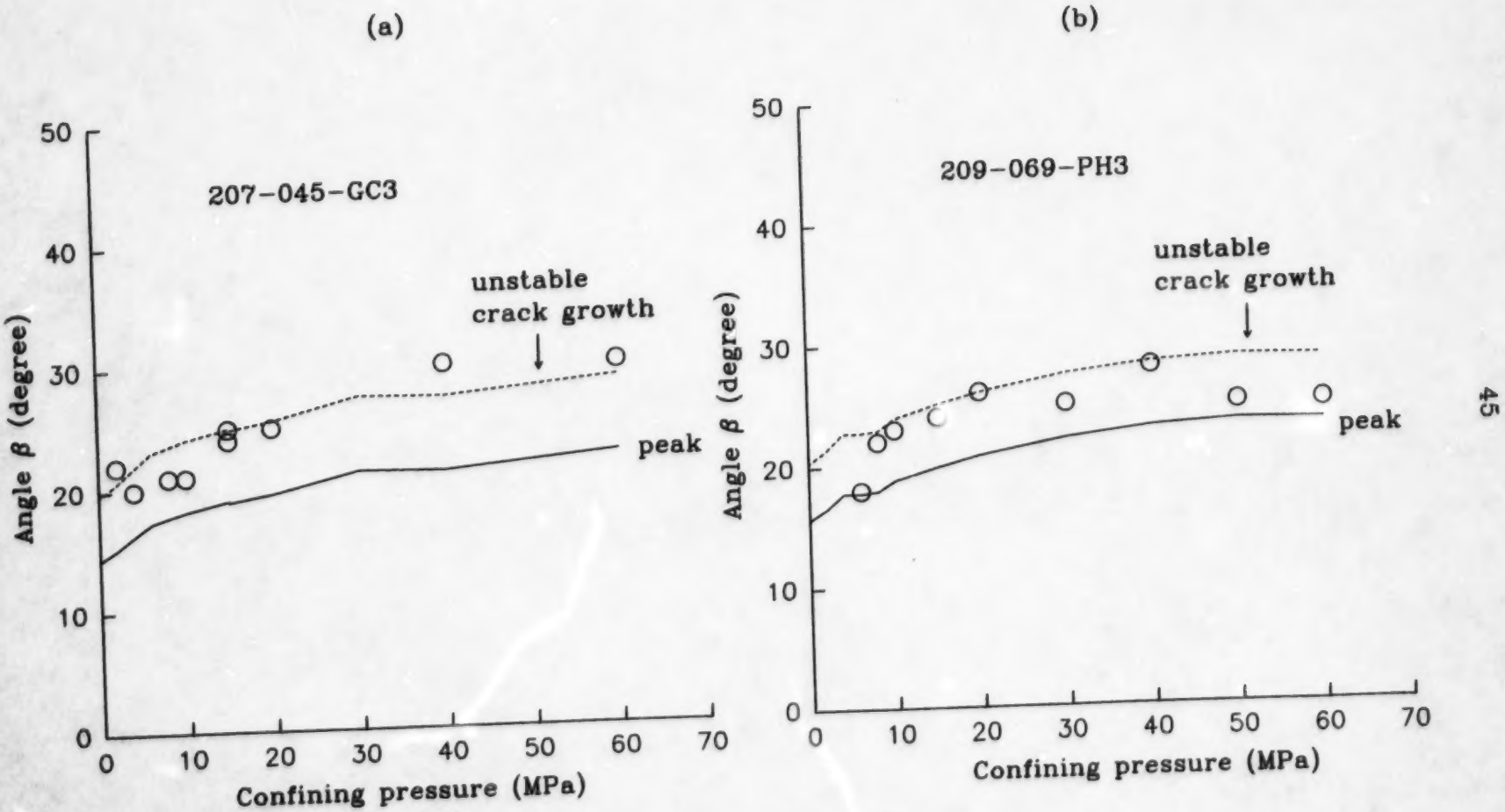

Figure 25. Plots of angle β versus confining pressure.

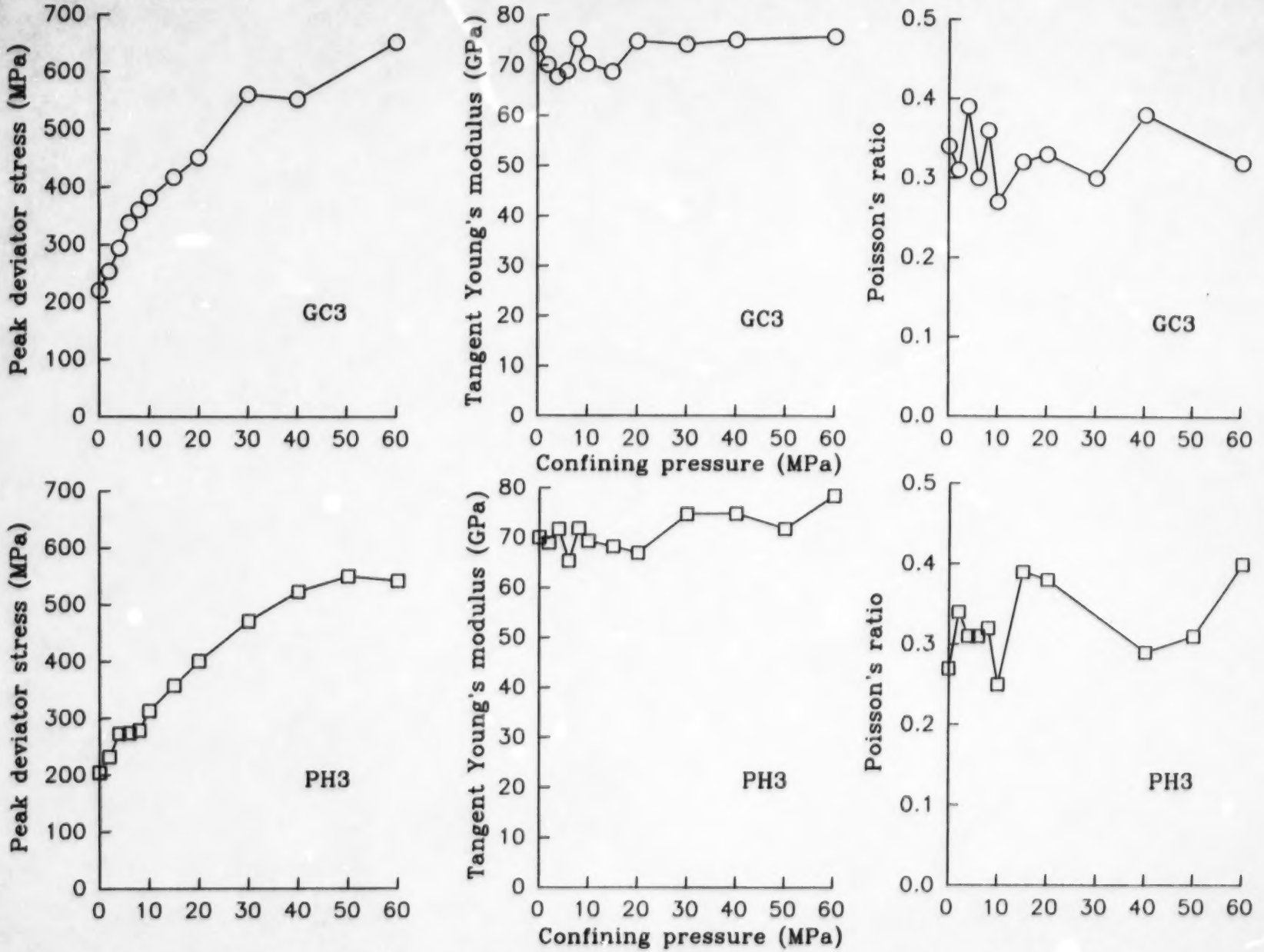

Figure 26. Effects of confining pressure on peak deviator stress, Young's modulus and Poisson's ratio.